POLYMER PHYSICS AND COMPUTER MODELING OF POLYARYL ETHER (PAE)-BASED SUPERPLASTICIZERS

Nurdaulet Mukhtarov, B. Eng in Chemical Engineering

Submitted in fulfilment of the requirements for the degree of Master of Science in Chemical and Materials Engineering

NAZARBAYEV UNIVERSITY

School of Engineering and Digital Sciences
Department of Chemical and Materials Engineering
Nazarbayev University

53 Kabanbay Batyr Avenue,
Astana, Kazakhstan, 010000

Supervisor: Pr. Yanwei Wang
Co-supervisor: Pr. Almagul Mentbayeva

April 2023

DECLARATION FORM

DECLARATION

I hereby declare that this manuscript, entitled "*POLYMER PHYSICS AND COMPUTER MODELING OF POLYARYL ETHER (PAE)-BASED SUPERPLASTICIZERS*", is the result of my own work except for quotations and citations which have been duly acknowledged. I also declare that, to the best of my knowledge and belief, it has not been previously or concurrently submitted, in whole or in part, for any other degree or diploma at Nazarbayev University or any other national or international institution.

Signature of author:.....

Name: Nurdaulet Mukhtarov

Date: April 7, 2023

ABSTRACT

Superplasticizers play a significant role in concrete industry. They are the special type of chemical admixtures that reduce water-to-cement ratio, improve the workability of cement pastes, and have hydration retention capabilities. The novel type of superplasticizers, called polyaryl ether (PAE), is a special type of current state-of-the-art comb-like polycarboxylate ethers (PCEs). PAE is very similar to PCE, except for the backbone's chemical nature. The aromacity of backbone increases the stiffness of backbone chain, which results in different adsorption behavior that might improve the particle dispersion of cement pastes and their rheology. Molecular Dynamics is a powerful tool that can be used to determine the structure and dynamics of various materials and processes on atomic scale, including the conformations of comb-shaped copolymer polyelectrolyte in free solution and adsorbed chain states. Unfortunately, the computational research of PAEs has not been extensive. In this work, the influence of backbone rigidity on conformational properties in free solution and adsorbed states of comb-like polyelectrolytes was studied by Coarse-Grained Molecular Dynamics simulations using the common structure of PCEs. Three comb configurations were constructed, each having different structural parameters n, N, and P. The simulations were performed in NVT ensemble with implicit solvent and explicit counterion methods. The results showed that radius of gyration of the comb in free solution gradually increases with the stiffness of the backbone and reaches a plateau at high rigidity. Moreover, the backbone flexibility affected the surface occupational area. The more rigid chains covered the more surface. The adsorption layer thickness was not affected by backbone flexibility when combs were fully adsorbed on the surface. These results coincided with polymer physics theories developed by Flatt et al., (2009) and Wang et al., (2018). Additionally, the grafting density affected the adsorption layer thickness. Comb configuration with lower N (higher grafting density) yielded smaller adsorption layer thickness, which could be due to stronger steric effect between adjacent sidechains. Observation of simulation snapshots revealed the influence of backbone charge density on the adsorption. Copolymers with lower charge density took longer time to adsorb on the surface due to weaker electrostatic interactions between backbone and surface.

Keywords: superplasticizers, polyaryl ether (PAE), backbone stiffness, comb-like polymer, polymer physics, computer simulation, adsorption, conformation

ACKNOWLEDGEMENTS

First of all, I would like to express my uttermost gratitude and appreciation towards my supervisors Pr. Yanwei Wang and Pr. Almagul Mentbayeva, who have helped me on this journey to successfully complete the master's program. I am appreciative for all the support and encouragement I received that motivated me to become a better student, as well as all the hours of discussion and constant feedback on my progress. Thank you for teaching me the methods of computational analysis on materials and polymers. I really hope this knowledge will carry on with me in my future career.

This work was carried out with support from Grant Award Number 240919FD3925 under the "*Polymer Physics and Modeling of Polycarboxylate-based Superplasticizers*" project from Nazarbayev University.

We acknowledge the National Supercomputing Center in Shenzhen for providing computational resources for Molecular Dynamics Simulations on LAMMPS software.

Special thanks to my friends Birzhan Abdikhan and Aigerim Kabulova for their constant support and peer-review.

Lastly, I thank my family for their loving support and faith in me.

TABLE OF CONTENTS

LIST OF ABBREVIATIONS & SYMBOLS

ALT – adsorption layer thickness

LS – lignosulfonate

MD – molecular dynamics

MPPEG – methylphenyl oxy PEG

PAA – polyacrylic acid

PAE – polyaryl ether

PCE – polycarboxylate ether

PCS – polycondensate sulfonate

PEG – polyethylene glycol

PMAA – polymethacrylic acid

PMS – polymelamine sulfonate

PNS – polynaphtalene sulfonate

$\mathbf{R_g}$ – radius of gyration

$\mathbf{S_A}$ – surface occupation area

SMD – small molecule dispersant

SP – superplasticiser

LIST OF FIGURES & TABLES

CHAPTER 1 – INTRODUCTION

1.1 GENERAL INTRODUCTION

Plasticizer is a type of chemical admixture that can reduce the yield stress or increase the plasticity of a material to which it is added. When the plasticizer is mixed with cement, it decreases a water-to-cement (W/C) ratio, which indicates the fraction of required water in cement paste. The excess water can lead to a formation of pores in cement structure due to partial water evaporation after the cement is cured. This leads to a compromise of cement's structural integrity[1]. A special type of plasticizer is called superplasticizer (SP), which can reduce W/C ratio up to 30-40%. They became popular after 1960s in Japan, Germany, and North America. Superplasticizers can increase the fluidity of cementitious materials by inducing a dispersion of cement particles due to adsorption on cement surface[2]. Additionally, current state-of-the-art superplasticizers can delay the hydration reactions occurring in various cement phases. Hydration increases the yield stress of cement due to formation of crystal phase due to diffusion of Ca^{2+} that leads to a hardening of concrete. Usually, it takes up to 24 hours for a decent hydration to occur, which might hinder the workability of cement pastes in some instances. However, by adding the superplasticizers, the hydration can be delayed up to 50 hours, thus improving the workability of cement paste[3] (Fig. 1.1).

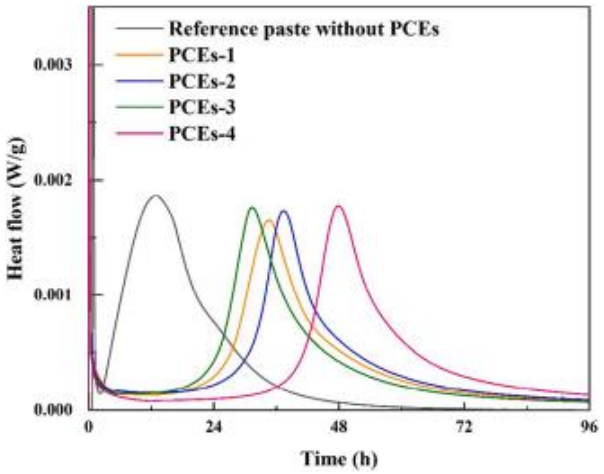

Figure 1.1 The retardation of hydration by polycarboxylate ethers (PCEs) in Portland cement[3].

1.1.1 LIGNOSULFONATE SUPERPLASTICIZERS

Depending on the type of superplasticizer, the cause of particle dispersion can hold either electrostatic repulsion or steric hindrance nature. There are three major SPs that have been used in concrete industry: lignosulfonates (LS), polycondensate sulfonates (PCS), and

polycarboxylate ethers (PCE). The former (LS) consists of phenylpropane with hydroxyl, methoxy, and sulfonic acid functional groups (see Fig. 1.2). The sulfonic acid group acts as an anchor and adsorbs on a positively charged site of cement surface, which predominantly consists of calcium ions (Ca^{2+}). A high density of negative charges from aromatic phenyl groups also contributes to the adsorption. The adsorption of several polymer chains leads to a reduction of positive charges and relative increase of negative charges, which results in negatively charged particles that repel each other electrostatically[4].

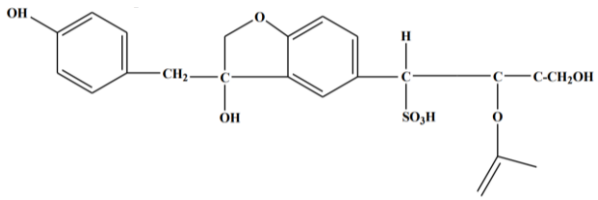

Figure 1.2 The chemical structure of lignosulfonate superplasticizer[4].

However, although lignosulfonates are the cheapest admixtures among other superplasticizers, the water reducing ability showcases only up to 10%, which hinders its use for high-performance concrete[5].

1.1.2 POLYCONDENSATE SUPERPLASTICIZERS

Polycondensate sulfonates are considered as the 2nd generation of SPs, after lignosulfonates. There are two common compounds: polynaphthalene sulfonate (PNS) and polymelamine sulfonate (PMS). Similar to lignosulfonates, both PNS and PMS have aromatic and sulfonic acid functional groups that induce the adsorption of SPs on the cement surface (refer to Fig. 1.3), implying the same mechanism of particle dispersion due to electrostatic repulsion[4].

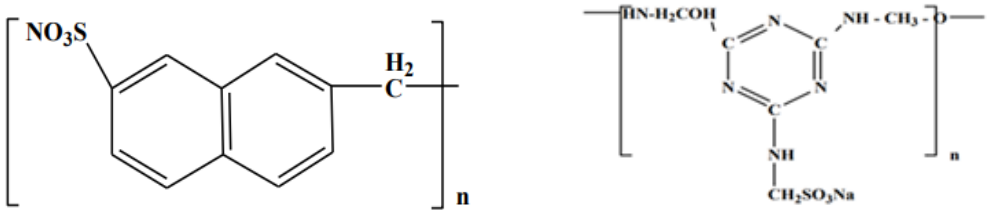

Figure 1.3 The chemical structures of PNS and PMS[4].

The PMS reportedly showed lower hydration retention capability along with higher slump loss[1]. Coupled with environmental issues, namely the formation of formaldehydes after cement hydration, the requirement for a more sustainable and effective alternative was raised[6].

1.1.3 POLYCARBOXYLATE ETHER SUPERPLASTICIZERS

The above-mentioned superplasticizers have a common limitation, which is an obstruction of air that may compromise the mechanical strength of concrete[7]. However, this was resolved when the current state-of-the-art superplasticizers, named polycarboxylate ether (PCE)-based SPs, were introduced. The crucial difference between PCE and previous SPs is the comb-like polymer chain structure[1]. The main backbone is aliphatic (PAA or PMAA) with anionic carboxylate groups, which adsorb on the surface of cement, whereas the sidechains (PEG) are neutral and induce a steric hindrance between the sidechains of adjacent PCE molecules (Fig. 1.4). The aliphatic nature of the backbone may compromise the adsorption of PCE onto cement particle due to the backbone being flexible. Despite that, the steric hindrance causes a better dispersion than previous SP generations, which results in reduced water requirement and enables an escape of air bubbles.

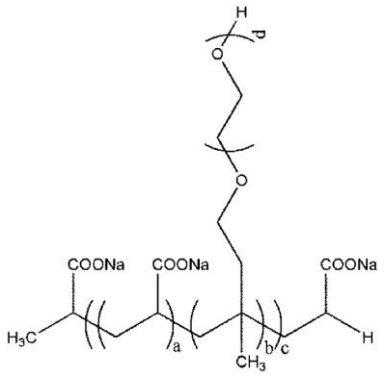

Figure 1.4 The chemical structure of polycarboxylate ether comb[8].

Despite being state-of-the-art, PCEs still have several limitations. Some PCEs can disturb the chemical balance of hydration, which might compromise the structural integrity of cured concrete. For example, it was reported that PCEs are sensitive to sulfates, which might cause foaming of solution, leading to increased porosity of cured concrete. Additionally, PCEs generally worked poorly with cements containing high clay content[3]. To overcome such issues, many tried modifying the molecular structure of PCE chains and/or changing the functional groups on the backbone. For instance, changing the conventional comb-like structure to star-comb shape resulted in higher retention effect and particle separation effectiveness, whereas PCEs based on cyclodextrin exhibited tolerable performance with clay[9]. In addition, the increase in backbone rigidity showed better PCE adsorption on cement surface[10]. It was shown that the conformation of more rigid PCE

backbone varied less in pore solution than in free solution, which is preferable for better adsorption[11].

1.1.4 POLYARYL ETHER SUPERPLASTICIZERS

Another approach is to change the production reaction mechanism from free radical polymerization to polycondensation. Recently, a novel type of superplasticizers called polyaryl ether (PAE) SP has emerged. Similar to PCEs, PAEs have comb-like copolymer structure with etheric sidechains, usually PEG. However, they have aromatic backbone, instead of aliphatic. It can be assumed that PAE is a combination of PCE and previous generation SPs.

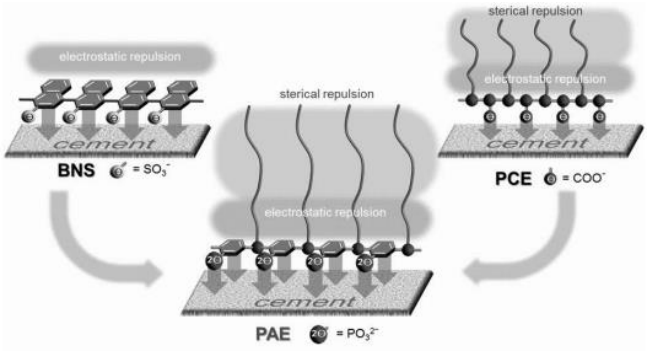

Figure 1.5 Schematic sketch of the structure and interaction mechanism of superplasticizers[12].

The aromatic nature of the backbone reduces the flexibility of main chain, which can affect the adsorption behavior. The higher rigidity of PAE backbone increases the adsorption extent compared to flexible PCE backbone, the latter of which may entrap anionic groups in polymer coil[9]. However, they are more exposed in PAEs due to backbone being stretched, which increases the number of available bindings (refer to Fig. 1.6). Thus, PAEs might have stronger and more stable adsorption. Li et al. studied the adsorption of copolymers on cement surface[9]. Fig. 1.7 shows the difference between the adsorbed amounts of PCEs and PAEs at various dosages and times after mixing. The amount of PAEs adsorbed on the surface is seemingly higher in comparison to PCEs at the whole range of dosage and time after mixing.

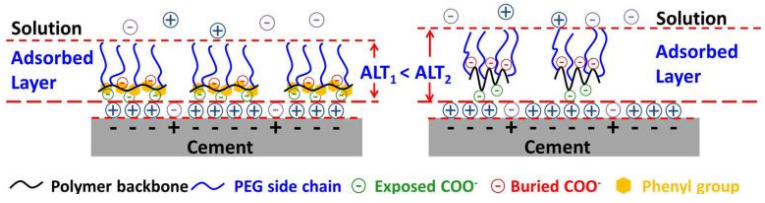

Figure 1.6 The adsorbed single chain of PAE and PCE[9].

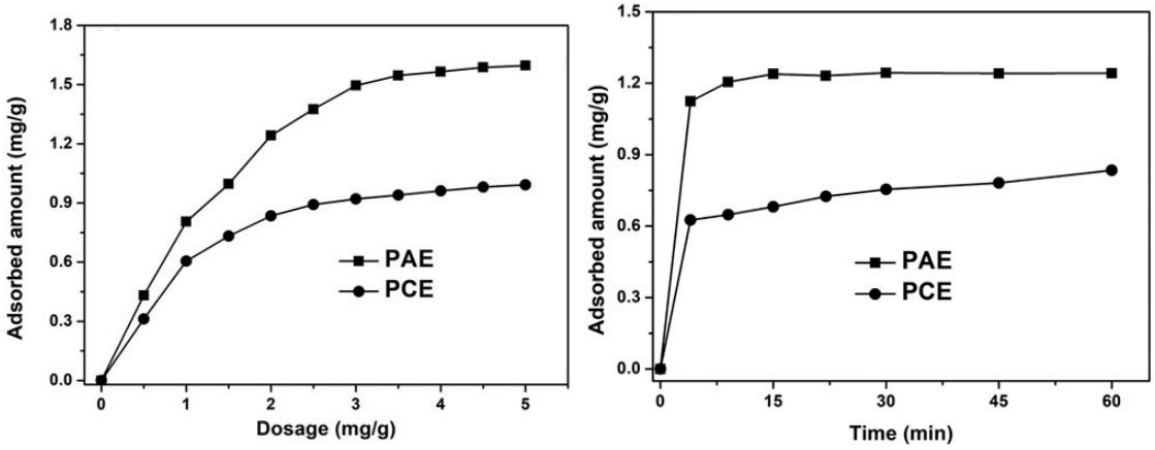

Figure 1.7 The adsorption extent of PCE and PAE depending on dosage (left) and time after mixing (right)[9].

Additionally, the authors studied the compatibility of PAEs with clays in cement[9]. It was found that PAEs had higher tolerance to the clay content in the cement than PCEs. The addition of 1 w% clay reduced the paste flow in both cases. However, the reduction was by only 26.9% for PAEs, which is considerably lower than 50.6% reduction with PCEs. The same tolerance was noticed with polycondensate SPs[13-14]. The study speculated that the similarity of PAE backbone with polycondensate SP structure could result in a similar outcome.

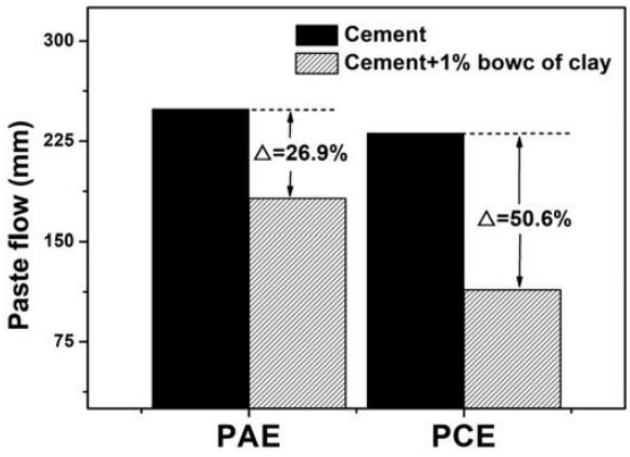

Figure 1.8 The comparison of paste flow between bare cement and cement with clay with PCE and PAE[9].

PAEs can delay the hydration of cement, similar to PCEs, possibly due to formation of chelates that inhibit the hydration reaction[15]. However, it was shown that the hydration retention by PAEs could be better than by polycarboxylates. In the same study, the heat flow analysis revealed that the cement mixed with PAEs resulted in higher hydration delay with initial and final setting times being approximately 90 minutes longer than that of PCEs[9] (Fig. 1.9).

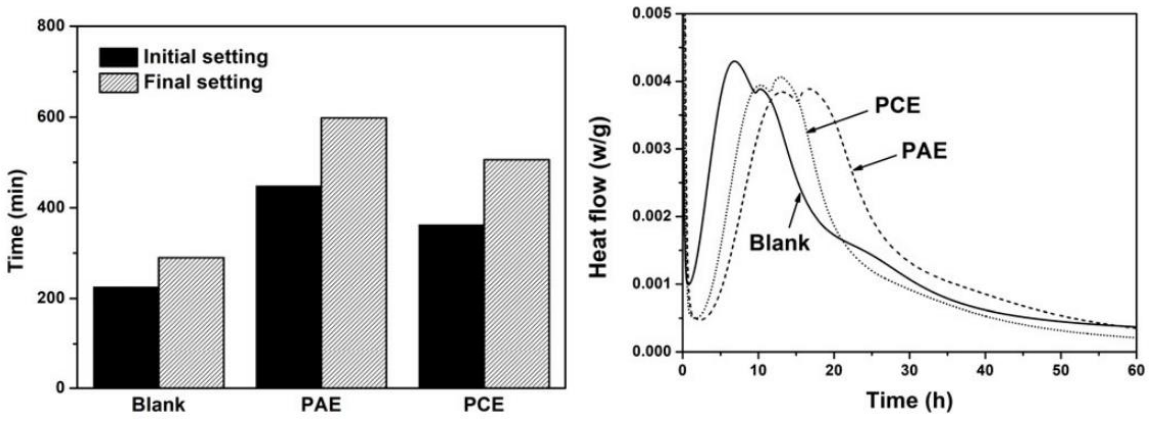

Figure 1.9 The setting time of cement with and without clay mixed with PCE and PAE[9].

The inventors of commercial PAE product, named MasterEase, conducted a set of experiments to determine the effect of PAEs on cement rheology and workability using V-funnel and L-box tests[12]. Fig. 1.10 illustrates the slump flow and funnel flow behaviors of PCE, PAE, and SMD, the latter of which refers to a small molecule dispersant that is the same single sidechain of the PCE with anionic functional groups. The results revealed that cement with PAE had a consistent workability in a duration of 30 minutes, whereas the one with PCE started losing its flowability after 10 minutes. The V-funnel experiment showed that cement mixed with PAE had the funnel flow time twice lower than that of PCE.

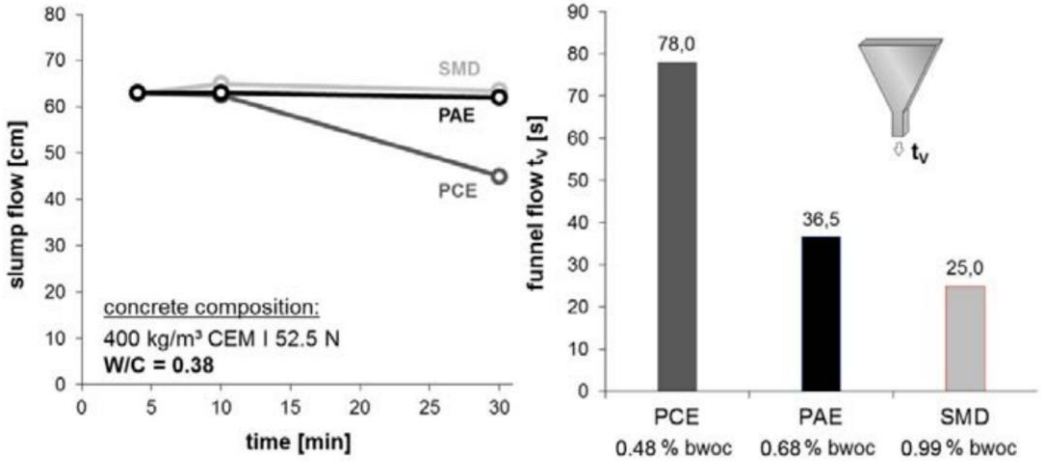

Figure 1.10 The slump (left) and funnel (right) flow behaviors of PCE and PAE[12].

Additionally, Fig. 1.11 depicts the apparent viscosities of cement pastes mixed with PCE, PAE, and SMD at constant initial slump flow and constant shear stress[12]. The viscosity measurements were made 400 s after the slump flow measurement, and results showed that cement with PAE was still less viscous than that of PCE. Interestingly, the apparent viscosity was the same between PCE and PAE at constant yield stress. This could indicate the certain effect of PAE on the thixotropy of the cement, which is the rheological

parameter that indicates the ability of soft matters to retain the equilibrium viscosity after it was gradually reduced by shear forces. The authors concluded that PAE possibly reduced the thixotropy of cement, which resulted in lower apparent viscosity compared to PCE after a certain amount of time.

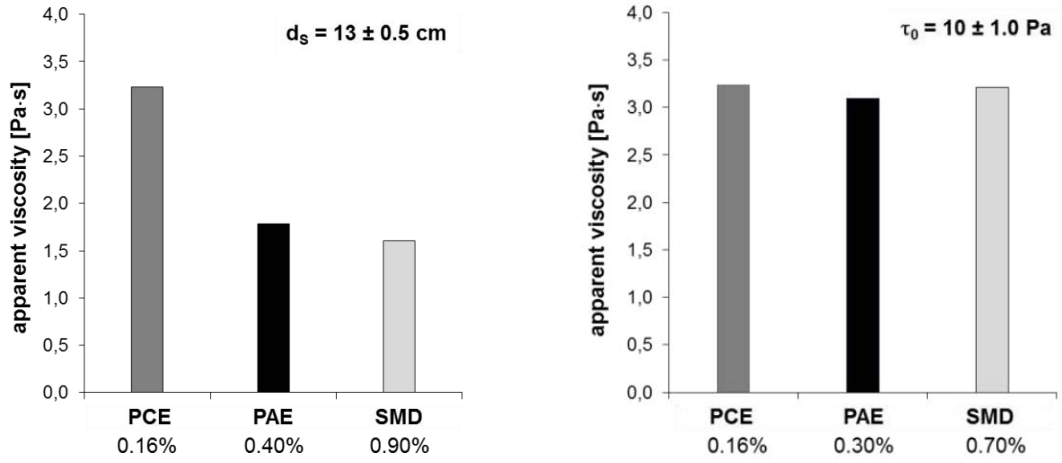

Figure 1.11 The apparent viscosities of cement pastes at constant slump flow (left) and constant shear stress[12].

Fig. 1.12 shows the correlation between shear stress and time at rest for PCE, SMD, and PAE at constant shear rate of 0.5 s^{-1} [12]. According to results, the shear stress of cement with PCE had the highest shear stress after 120 s, whereas that of PAE had the lowest. This implies the same conclusion the authors made about the reduction of thixotropy after addition of PAE. Moreover, the visual observations showed that cement pastes with PAEs were generally less sticky than those with PCEs. This is significant, as stickiness increases the pump load, which reduces the sustainability of construction and increases the operation cost.

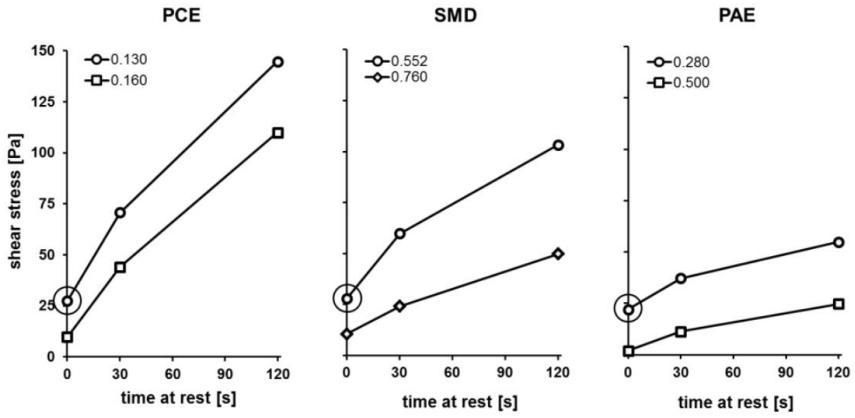

Figure 1.12 The shear stress of cements with PCE, SMD, and PAE at various times at rest[12].

1.1.5 COMB LIKE POLYMER MODEL FOR PCES AND PAES

The dispersion of particles depends on two main factors: chemical nature and molecular structure. There are many kinds of PCEs available at the market, but most commonly the sidechains are made of polyethylene glycols (PEGs). The backbone is typically made of aliphatic polyacrylic (PAA) or polymethacrylic acid (PMA) monomers with anionic functional groups (also referred to as anchors). As its name suggests, PCE has carboxylic groups that provide negative charges in backbone. However, there could be other functional groups, such as phosphonic and sulfonic. The choice of anchors depends on the type of application. In case of PAEs, the sidechains can be of the same material, but the backbone is no longer aliphatic. Instead, it is aromatic and could be created by a polycondensation reaction between salicylic acid, *p*-methylphenyl oxy PEG (MPPEG) and paraformaldehyde, using the concentrated sulfuric acid as catalyst[9]. The anionic anchors can be either carboxylic or phosphonic.

The diversity of chemical nature is low compared to the variability of molecular structure. The molecular structures of the same superplasticizer product may vary, depending on the method of synthesis. There are three main factors that determine the molecular structure: backbone length, sidechains length, negative charge density and grafting density. The number of backbone monomers affects the size of the backbone and the charge density, whereas the number of sidechain monomers determines the length of sidechains. Although the experimental studies had shown the feasibility of superplasticizers, the theory behind dispersion and adsorption physics was uncertain. The convenient way of establishing the physical theory was to come up with a simple molecular structure model. The common model was derived by Gay and Raphael in 2001[16], which was later used in many theoretical studies, including Flatt et al. (2009) and Wang et al. (2018)[17-18] (Fig. 1.13). Refer to Chapter 2 of this thesis to find further details about these two theories.

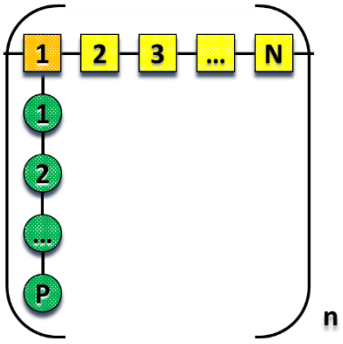

Figure 1.13 Gay and Raphael model of comb-like copolymers[16].

In this model, the monomers in backbone and sidechains are represented by blobs: yellows refer to backbone and greens refer to sidechains. The orange blob is a connector between backbone and sidechains and is uncharged. Therefore, for a comb with n sidechains, there are N backbone monomers between adjacent sidechains and P sidechain monomers. Using this structural model, the conformations of comb copolymers in dilute solution and in instances of complete adsorption can be modeled and quantitatively studied.

1.2 MOLECULAR DYNAMICS SIMULATIONS

Molecular Dynamics (MD) is a classical method to find information about dynamics and structure of materials on atomic scale. The atoms are represented by solid balls, whereas the chemical bonds are depicted by a physical spring, therefore being referred to as spring-and-ball model (Fig. 1.14). The interactions between atoms are well-established by many simulation studies and ab initio calculations. Depending on the nature of interaction, the atoms have various force fields, through which they either attract or repel each other. These forces are induced by so-called potentials that ultimately decide the movements of atoms. The idea behind molecular dynamics is to calculate the forces acting on atoms using said potentials, let the atoms move due to induced forces for a very little increment of time, and to calculate the forces on new positions. The process usually continues until the system reaches its equilibrium. Using the information about the position, velocity, and forces, it is possible to calculate the transport and thermodynamic properties of materials.

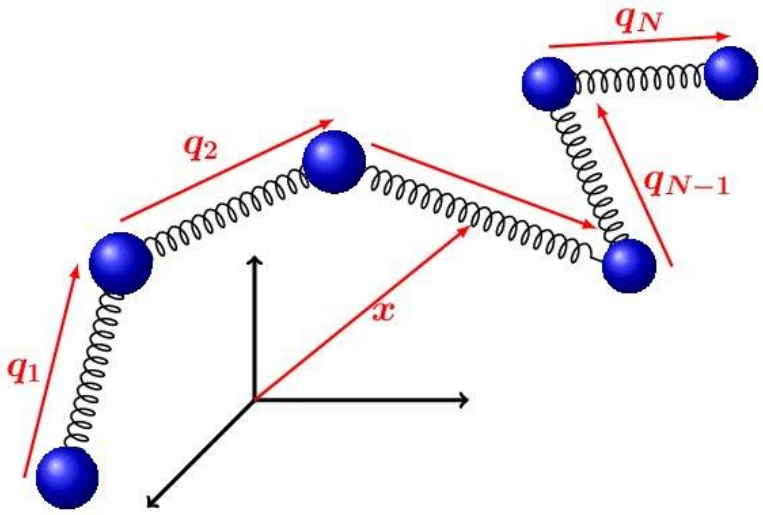

Figure 1.14 The polymer chain depicted by the spring-and-ball model[19].

1.2.1 FORCE FIELDS & INTERATOMIC POTENTIALS

The common force fields used to simulate surfactants, polymers and other various materials combine into a group called Class I force fields. It includes such force fields as Amber, GROningen MOlecular Simulation (GROMOS), Chemistry at HARvard Macromolecular Mechanics (CHARMM), and others. Despite the variety of the models, they all have the same functional form, depicted below:

$$E = \sum_{bonds} K_b(b - b_0)^2 + \sum_{angles} K_\theta(\theta - \theta_0)^2 + \sum_{dihedrals} K_{\phi,n}[1 + \cos(n\phi - \delta_n)] + \sum_{impropers} K_\phi(\phi - \phi_0)^2 + \sum_{i \neq j} \left(\frac{q_i q_j}{r_{ij}}\right) + E_{LJ} \quad \text{Eq. 1.1}$$

which can be simplified as follows:

$$E = E_{bonded}(\boldsymbol{r}) + E_{non-bonded}(\boldsymbol{r}) \quad \text{Eq. 1.2}$$

The bonded term includes the bond, angle, dihedral, and improper dihedral potentials, whereas non-bonded term consists of Lennard-Jones and Coulomb potentials. The latter two are also referred to as van der Waals and electrostatic interaction potentials, respectively. Typically, they have the following governing equations:

$$V_{LJ}(r) = 4\varepsilon\left(\left(\frac{\sigma}{r}\right)^{12} - \left(\frac{\sigma}{r}\right)^{6}\right) \quad \text{Eq. 1.3}$$

$$V_{Coul}(r) = \frac{q_i q_j}{4\pi\epsilon_0 r_{ij}} \quad \text{Eq. 1.4}$$

where V_{LJ} = the LJ potential, r = the distance between paired particles, r_c = the cutoff distance, ε = the well depth, and σ = the particle size; V_{Coul} = the Coulomb potential, q_i, q_j = the particle charges, r_{ij} = the distance between particles i and j, and ϵ_0 = the vacuum permittivity.

1.2.2 BOUNDARY CONDITION

The simulation box may have either periodic or non-periodic walls. If the walls are periodic in all dimensions, the simulation box is considered as the smallest unit of the infinitely large environment, consisting of the same box, meaning that a particle crossing the wall appears from the opposite side of the box. This creates the illusion of a big system, while the calculations are performed on the actual simulation box. The size of the simulation box must be carefully determined before the simulation. If the size is too small, the molecule inside the box can interact with the molecule in an adjacent box, which is

impractical when e.g. simulating a single molecule in free solution. On the other hand, if the simulation box is too large, the false interactions may disappear, but the computational cost increases. It is possible to have non-periodic walls in one direction while others are periodic. Such cases are mostly used when simulating interface phenomena, such as adsorption.

1.2.3 THERMODYNAMIC ENSEMBLES

Thermodynamic ensembles define the thermodynamic state of the system during simulations. There are four main thermodynamic ensembles: microcanonical (NVE), canonical (NVT), grand-canonical (μVT), and isobaric-isothermal (NPT) ensembles. The letters in the abbreviations refer to the thermodynamic parameters that are held constant during the simulation: number of atoms/particles in the system (N), volume of the system (V), energy of the system (E), chemical potential of the system (μ), pressure of the system (P), and temperature of the system (T). Each ensemble resembles a certain thermodynamic state. For instance, the microcanonical ensemble (NVE) describes isolated systems with constant number of atoms, volume, and energy. In canonical ensemble (NVT), the temperature is held constant instead of energy, thus resembling a closed system in heat bath at constant temperature. The grand-canonical ensemble (μVT) describes open systems at constant temperature, as the number of atoms may change, and isobaric-isothermal (NPT) depicts the system with constant pressure and temperature.

1.2.4 SIMULATION TIMESTEP & COARSE-GRAINED MD SIMULATIONS

The simulation timestep is essentially an increment of time, required to calculate new velocities and accelerations from numerical integrations. Careful evaluation is necessary when choosing the appropriate timestep. The shorter the timestep, the more accurate depiction of the system can be obtained. However, this increases the computational cost. On the other hand, the longer timestep may enable simulations of system for longer times (more than several nanoseconds), but the accuracy might be compromised. Moreover, this may cause the overlapping of atoms, which leads to errors due to infinite forces. Generally, the timestep is set as 1 fs (or 10^{-15} s).

Many studies implemented the all-atom MD simulations to examine the conformation of PCEs in free solution and in adsorbed states, coupled with the interactions between solvent phase and cement phase[11,20-26]. Unfortunately, the PAEs have not yet been studied as thoroughly as PCEs using MD simulations. This is because the chemical structure of PAEs is only vaguely known from patents[27]. However, considering that PCEs

and PAEs have similar comb structure, it is possible to adapt polymer physics theories and MD simulation models to PAEs based on PCE studies. Therefore, all relevant PCE studies are beneficial for this research.

The adaptation requires the application of coarse-graining, which is a method of simplifying the group of atoms into a single blob. This concept is similar to Gay and Raphael's model of comb structure. The main advantage of coarse-graining over all-atom MD is that the computational cost is greatly reduced. The ab initio (first principles) molecular dynamics simulations provide high accuracy data on polymer conformation and thermodynamics. However, considering the total number of atoms in a single comb, free ions, surface ions and solvent, the cost of computation could be expensive. Therefore, the comb copolymer can be coarse-grained, maintaining the same structure as in Gay and Raphael's model. Moreover, the cost can be further reduced by using implicit solvent method, which uses the specified permittivity of the solvent instead of actual solvent molecules. Another advantage of such simplification is that the monomers are represented by blobs that have the same mass and size. Thus, the same comb configuration can be applied to both PCEs and PAEs, the only distinguishing parameter being the bending modulus (or stiffness) of the backbone.

Although coarse-graining greatly reduces the computational cost, the accuracy of results can be compromised by simplified interaction models. Additionally, the persistence length of PAE backbone has not been documented, thus the arbitrary bending modulus values were used during MD simulations.

1.3 OBJECTIVE OF THESIS

This thesis aims to:

- examine how existing PCE polymer physics theories apply to PAEs using the Gay and Raphael structural model;
- simulate comb-like copolymer with various backbone flexibility using coarse-grained Molecular Dynamics Simulations;
- study the effect of backbone stiffness on comb conformations in free solution and in adsorbed single chain states.

The main PCE polymer physics theories were Flatt et al. (2009) and Wang et al. (2018) models, where the former is based on the scaling law approach and the Helmholtz free energy minimization, and the latter is on the Wormlike Chain (WLC) model. The key

conformation parameters were the Radius of Gyration (R_g), the Adsorption Layer Thickness (ALT), and the Surface Occupation Area (S_A).

1.4 STRUCTURE OF THESIS

The structure of this thesis is organized into five main chapters. Chapter 1 provides a general introduction to the research topic, highlighting its significance and research questions or hypothesis. Chapter 2 presents a comprehensive literature review of the existing studies related to the research topic, identifying gaps and areas for further research. In Chapter 3, theoretical derivations are presented, which describe the theoretical foundation of the research and provide a detailed explanation of the research methodology. Chapter 4 presents computer simulations that were conducted to test the theoretical predictions and validate the research findings. Finally, in Chapter 5, a summary of the main results is presented, and the conclusions are drawn, along with suggestions for future research.

CHAPTER 2 – LITERATURE REVIEW

2.1 THEORETICAL MODELS

In this chapter, two polymer physics theories by Flatt et al. (2009)[17] and Wang et al., (2018)[18] are presented, along with MD simulations and computational studies on PCEs.

2.1.1 FLATT ET AL. (2009) THEORY: FREE SOLUTION CONFORMATION

According to Flatt et al. (2009), the conformation of the comb copolymer in free solution can be described by its radius of gyration. From the Helmholtz free energy minimization, the radius of gyration can be derived as follows:

$$R_g(n,N,P) = \left(\left(\frac{a_N}{a_P}\right)^2 \frac{(1-2\chi)}{2}\right)^{1/5} a_P P^{2/5} N^{1/5} n^{3/5} \quad \text{Eq. 2.1}$$

where a_N and a_P are the backbone and sidechain monomer sizes (0.25 and 0.36 nm, respectively), χ is the Flory parameter (0.37 for PEO at 25 ºC), N, P and n are the number of backbone and sidechain monomers and the number of repeating segments, correspondingly.

2.1.2 FLATT ET AL. (2009) THEORY: ADSORBED STATE CONFORMATION

Flatt et al. (2009) reported that the adsorption layer thickness corresponds to the radius of the hemisphere that bounds adsorbed cores:

$$R_{AC}(n,N,P) = \left(2\sqrt{2}(1-2\chi)\frac{a_P}{a_N}\right)^{1/5} a_P P^{7/10} N^{-1/10} \quad \text{Eq. 2.2}$$

According to the equation above, the adsorption layer thickness does not depend on n, which is reasonable because a change in the number of repeating segments does not alter the length of sidechains or the fraction of charged blobs ρ_e in the backbone. On the other hand, the number of monomers in each section determines the fraction of charged blobs according to the following equation:

$$\rho_e = \frac{N-1}{N} \quad \text{Eq. 2.3}$$

Hence, the longer each section is, the higher is the fraction and the stronger is the adsorption. At low fraction of charged blobs, the adsorption could be weaker, which might

cause an incomplete backbone adsorption or even backbone entanglement, which increases the adsorption layer thickness. Thus, there is a negative power index to N. Moreover, the number of monomers in sidechains directly determines the adsorption layer thickness, especially in the case of complete adsorption, in which it is reasonable to assume that the layer thickness would equal the average radius of gyration of sidechains.

The surface occupation area of the adsorbed chain can be determined as follows:

$$S_A(n,N,P) = \frac{\pi}{\sqrt{2}} a_N a_P \left(2\sqrt{2}(1-2\chi)\frac{a_P}{a_N}\right)^{2/5} P^{9/10} N^{3/10} n \qquad \text{Eq. 2.4}$$

According to the equation above, the surface occupation area is strongly related to the number of segments and the number of monomers in sidechains. Reasonably, the longer chain occupies the larger surface. Similarly, the longer sidechains block the wider area of the adsorption surface. According to the theory by Flatt et al. (2009), the surface occupation area of the single chain in the cases of single adsorbed chain and densely packed configurations would be the same due to neglecting of the excluded volume phenomena.

2.1.3 WANG ET AL. (2018) THEORY: FREE SOLUTION CONFORMATION

According to Wang et al. (2018), the conformation of the comb copolymer worm can be described via its radius of gyration, which is a function of 5 structural parameters:

$$\langle S^2 \rangle = \Phi(L_{bb}, l_{bb}; L_a, l_a; n) \qquad \text{Eq. 2.5}$$

$$\langle S^2 \rangle = \langle S^2 \rangle_m + \langle S^2 \rangle_s \qquad \text{Eq. 2.6}$$

$$\langle S^2 \rangle_m = \left(\langle \widetilde{S^2} \rangle_{m1} + \langle \widetilde{S^2} \rangle_{m2} + \langle \widetilde{S^2} \rangle_{m3}\right) \frac{L_{bb}^2}{L_T^2} \frac{L_{bb} l_{bb}}{3} \qquad \text{Eq. 2.7}$$

$$\langle \widetilde{S^2} \rangle_{m1} = 1 - \frac{3}{n_{bb}} + \frac{6}{n_{bb}^2} - \frac{6}{n_{bb}^3}(1 - e^{-n_{bb}}) \qquad \text{Eq. 2.8}$$

$$\langle \widetilde{S^2} \rangle_{m2} = 3n \frac{L_a}{L_{bb}} \left[\frac{2n+1}{3(n+1)} - \frac{2}{n_{bb}} + \frac{4}{n_{bb}^2} - \frac{4e^{-n_c}}{n_{bb}^2 n}\left(\frac{1-e^{-n_c n}}{1-e^{-n_c}}\right)\right] \qquad \text{Eq. 2.9}$$

$$\langle \widetilde{S^2} \rangle_{m3} = \frac{L_a^2}{L_{bb}^2} \left[\left(1 - \frac{3}{n_{bb}}\right)(n-1)n + \frac{6e^{-n_c}}{n_{bb}(1-e^{-n_c})}\left(n - \frac{1-e^{-n_c n}}{1-e^{-n_c}}\right)\right] \qquad \text{Eq. 2.10}$$

$$\langle S^2 \rangle_s = \left(\langle \widetilde{S^2} \rangle_{s1} + \langle \widetilde{S^2} \rangle_{s2}\right) \frac{L_a^2}{L_T^2} \frac{L_a l_a}{3} n \qquad \text{Eq. 2.11}$$

$$\langle \widetilde{S^2} \rangle_{s1} = 1 - \frac{3}{n_a} + \frac{6}{n_a^2} - \frac{6}{n_a^3}(1 - e^{-n_a}) \qquad \text{Eq. 2.12}$$

$$\langle \widetilde{S^2} \rangle_{s2} = 3\left(\frac{L_T}{L_a} - 1\right)\left[1 - \frac{2}{n_a} + \frac{2}{n_a^2}(1 - e^{-n_a})\right] \qquad \text{Eq. 2.13}$$

$$L_T = L_{bb} + nL_a \qquad \text{Eq. 2.14}$$

$$n_a = \frac{L_a}{l_a} \qquad \text{Eq. 2.15}$$

$$n_{bb} = \frac{L_{bb}}{l_{bb}} \quad \text{Eq. 2.16}$$

$$n_c = \frac{L_c}{l_{bb}} = \frac{n_{bb}}{n+1} \quad \text{Eq. 2.17}$$

where L_{bb} and L_a are the backbone and sidechain contour lengths, l_{bb} and l_a are the backbone and sidechain persistence lengths, and n is the number of sidechains. The contour length of the backbone is the end-to-end distance of the fully stretched chain, which can be approximated as the sum of lengths of all backbone monomers:

$$L_{bb} = nNa_N \quad \text{Eq. 2.18}$$

The free solution backbone persistence length depends on the sum of bare (κ_{bare}), electrostatic (κ_{elec}), and steric (κ_{ster}) bending stiffnesses:

$$l_{bb} = \frac{\kappa_{bare} + \kappa_{elec} + \kappa_{ster}}{k_B T} = l_{bb,bare} + l_{bb,elec} + l_{bb,ster} \quad \text{Eq. 2.19}$$

The bare stiffness modulus is the stiffness of the linear chain in free solution. The electrostatic effect comes from the electrostatic repulsion between charged blobs in the backbone. The steric effect is the result of steric hindrance between grafted sidechains.

Sulatha and Natarajan computed the intrinsic persistence length of PMAA chain from their simulation studies (0.64 nm)[28]. The influence of the charged backbone can be approximated as follows[29]:

$$\kappa_{elec} \approx 0.32(l_B/a_N)\rho_e^2 \lambda_D k_B T \quad \text{Eq. 2.20}$$

from which the "electrostatic" persistence length is derived:

$$l_{bb,elec} \approx 0.32(l_B/a_N)\rho_e^2 \lambda_D \quad \text{Eq. 2.21}$$

Here, l_B is the Bjerrum length, a_N is the backbone monomer size, ρ_e is the backbone charge fraction, and λ_D is the Debye length. Lastly, the steric effect can be expressed as follows[30]:

$$\kappa_{ster} \approx 0.04(L_a/L_c)^2 l_a k_B T \quad \text{Eq. 2.22}$$

where L_a is the contour length of the sidechains, l_a is the persistence length of the sidechains, and L_c is the backbone contour length between adjacent grafting points:

$$L_a = Pa_P \quad \text{Eq. 2.23}$$

$$L_c = L_{bb}/(n+1) \quad \text{Eq. 2.24}$$

Hence, the "steric" persistence length is:

$$l_{bb} \approx 0.04(L_a/L_c)^2 l_a \quad \text{Eq. 2.25}$$

Combining all expressions, the apparent persistence length of PMAA backbone becomes

$$l_{bb} = 0.64 + 0.32(l_B/a_N)\rho_e^2\lambda_D + 0.04(L_a/L_c)^2 l_a \quad \text{Eq. 2.26}$$

2.1.4 WANG ET AL. (2018) THEORY: ADSORBED STATE CONFORMATION

According to Wang et al. (2018), the surface occupation area of the single adsorbed chain can be estimated as follows:

$$\langle R^2\rangle_{bb,2D} = \begin{cases} 2l_{bb,2D}^2\left[\frac{L_{bb}}{l_{bb,2D}} + \exp\left(-\frac{L_{bb}}{l_{bb,2D}}\right) - 1\right] & L_{bb}/l_{bb,2D} \le 2.1491 \quad \text{Eq. 2.27} \\ 0.8035\, l_{bb,2D}^2\left(\frac{L_{bb}}{l_{bb,2D}}\right)^{3/2} & L_{bb}/l_{bb,2D} > 2.1491 \quad \text{Eq. 2.28} \end{cases}$$

$$S_A \approx \frac{\pi}{4}\langle R^2\rangle_{bb,2D} \quad \text{Eq. 2.29}$$

where $\langle R^2\rangle_{bb,2D}$ is the mean-square end-to-end distance of the adsorbed backbone, $l_{bb,2D}$ is the persistence length of the adsorbed backbone, L_{bb} is the contour length of the backbone and S_A is the surface occupation area. Wang et al. (2018) suggested that the persistence length of the adsorbed chain on a 2D plane becomes a double of that in free solution:

$$l_{bb,2D} = 2l_{bb} \quad \text{Eq. 2.30}$$

From the surface occupation area calculations, the adsorption layer thickness can be computed as follows:

$$H_{ads} \cong \begin{cases} 2R_{g,PEG} & \sigma \le \left(2R_{g,PEG}\right)^{-2} \quad (\text{Mushroom}) \quad \text{Eq. 2.31} \\ 0.7L_a(\sigma l_a^2)^{\frac{1}{3}} & \sigma > \left(2R_{g,PEG}\right)^{-2} \quad (\text{Brush}-\text{like}) \quad \text{Eq. 2.32} \end{cases}$$

where $R_{g,PEG}$ is the radius of gyration of the sidechain in dilute solution, L_a is the sidechain contour length, l_a is the sidechain persistence length, and σ is the local grafting density at low surface coverage:

$$\sigma \approx \frac{n}{S_A} \quad \text{Eq. 2.33}$$

The radius of gyration of PEG chain can be estimated from Benoit and Doty equation:

$$R_g^2 = b^2\left(\frac{L}{3b} + 1 + 2\left(\frac{b}{L}\right) - 2\left(\frac{b}{L}\right)^2\left(1 - \exp\left(-\frac{L}{b}\right)\right)\right) \quad \text{Eq. 2.34}$$

where L and b are the contour and persistence lengths of a linear chain, respectively. Rewriting the above equation in accordance with the current notation yields:

$$R_{g,PEG}^2 = l_a^2\left(\frac{L_a}{3l_a} + 1 + 2\left(\frac{l_a}{L_a}\right) - 2\left(\frac{l_a}{L_a}\right)^2\left(1 - \exp\left(-\frac{L_a}{l_a}\right)\right)\right) \quad \text{Eq. 2.35}$$

2.2 MOLECULAR DYNAMICS STUDIES OF PCES

The molecular dynamics studies on PCEs, primarily made to evaluate the influence of structural parameters and solvent interactions on the conformations of PCEs, play an important role in many PCE computational studies, because they provide the basic knowledge about spatial orientation of copolymers in free and pore solutions, which determine the adsorption behavior[31]. The experiments have shown the great effect of adsorption behavior on cement rheology[3,9-13,15]. The data from such studies can be compared with experimental results obtained from small-angle neutron scattering and light scattering to determine the appropriate force fields and interaction parameters for further studies. Moreover, although the solution conformation does not directly affect the cement rheology, the adsorbed conformation can be determined from the same polymer physics theories applied to solution conformations.

2.2.1 SOLUTION CONFORMATIONS

As discussed before, the main parameters that define the structure of the comb are the number of backbone monomers (N), number of sidechain monomers (P), and number of sidechains. Although the coarse-grained MD simulations do not give the most accurate results, they can be useful in quick assessment of chain conformations in both free solution and adsorbed states. Several studies have shown that with number of sidechain and backbone monomers, the equilibrium size or radius of gyration of comb chains increases[8,32-33]. Moreover, the number of sidechains can affect the size of the backbone due to steric hindrance between the sidechains[8,32]. The grafting density had notable effect on the free solution conformation too. At higher grafting density, the backbone was observed to be stretched due to steric effect between sidechains, which could increase the radius of gyration[8,32]. The charge density relates to the grafting density for the same copolymer with various comb configurations, so a similar impact can be observed[8,32-33].

Such parameters as backbone charge density and grafting density can be computed using those three parameters (see previous section).

Additionally, the solution pH and valency of counterions strongly determine the pore solution conformation due to electrostatic interactions. Atomistic MD simulations performed on linear PAA and combed PCE with PAA backbone have shown the impact of calcium, sodium, and chloride ions on their conformation. According to the results, the PAA chain without grafted sidechains easily coiled, in contrast to PCE. The calcium ions were prevented from coming closer to carboxylic groups due to strong steric hindrance provided by sidechains[34]. Another study investigated the free solution conformation PCEs with various grafting densities by changing the calcium concentration. It was found that the radius of gyration decreased for all configurations when calcium concentration raised. This could be due to shielding effect, caused by calcium ions, that decreased the electrostatic interaction between adjacent carboxylic groups[35]. This implies that the steric effect of sidechains can be overcome by high concentration of calcium ions.

The effect of the methyl group in the backbone has also been studied in the solution with calcium ions. The change from PAA to PMAA revealed that methyl groups decreased the stiffness of the backbone, yielding coiled PCE conformations. The authors also concluded that the addition of methyl groups increased the affinity of carboxylic groups towards calcium ions, which implies the higher capability to adsorb on charged surface[11]. This is in contrast with another study, where it was suggested that the extended backbone provides more anchors, since they may be entrapped in the coil of flexible backbone[9].

A more realistic study has been performed on three PCE types with different structures in water and pore solution with calcium, sodium, potassium, hydroxyl, and sulphate ions. The study provides more relevant and accurate data than previous findings, since the simulated pore solution resembles real life samples and the modelled PCEs have actual sizes and molecular weights. The results showed that PCEs were more extended in free solution due to steric hindrance, but the size reduced because of high ionic concentration[24].

2.2.2 ADSORBED CONFORMATIONS

The influence of structural parameters on the adsorption behavior has also been studied. Copolymers with shorter sidechains may yield more flexible backbones near the surface[20,22]. Moreover, atomistic molecular dynamics simulations on extended comb polyelectrolytes have shown that only a small fracture of charges on the middle section of

backbone interacts with the charges on the surface, while this value decreases for coiled conformations[36]. This implies that the surface occupational area should increase with the stiffness of backbone. Atomistic MD simulations have also shown how the initial orientation of combs affects the final conformation on the surface. The parallel or perpendicular position resulted in looped conformations, which had higher ALT[25]. All the studies were primarily focused on the adsorption energies. Some of them provided numerical values without comparison with experimental data, whereas others did not equilibrate the system in simulations, which could yield non-realistic results. Nonetheless, the simulation snapshots allowed to observe possible adsorbed state conformations of PCEs on cement surface. Still, more molecular dynamics studies are required to understand more about the impact of charge density, grafting density and backbone flexibility on surface occupation area, adsorption layer thickness and adsorption energy.

CHAPTER 3 – THEORETICAL DERIVATIONS

3.1 INTRODUCTION

In this section, the two models will be compared using the set of various PCE configurations, implemented in Flatt et al. (2009) study (Fig. 3.1). All configurations were in a so-called *Flexible Backbone Worm* (FBW) regime, in which the comb copolymers can be remodeled as a chain consisting of cores, each core containing several sidechains and a flexible backbone. Both Flatt et al. and Wang et al. theories can be applied to common comb like PCE structures in FBW regime. However, as the backbone becomes more rigid, the backbone stretches, which might cause the copolymer to shift towards *Stretched Backbone Worm* (SBW) regime. Ultimately, the goal of this chapter is to apply the introduced models to different comb configurations and to see how the backbone rigidity and charge density affect the results.

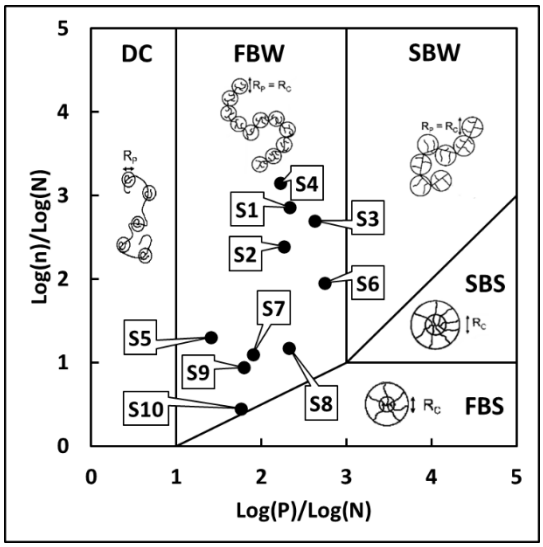

Figure 3.1 Phase diagram of comb copolymers. DC – Decorated Chain, FBW – Flexible Backbone Worm, SBW – Stretched Backbone Worm, SBS – Stretched Backbone Star, and FBS – Flexible Backbone Star. Black dots represent different PCE configurations fitted into the phase diagram.

3.2 METHODOLOGY

Flatt et al. and Wang et al. theories were compared on comb copolymer conformations in free solution and adsorbed single chain cases using a set of 10 comb configurations used in Flatt et al. (2009) work. The summary of comb configurations is provided in Table 3.1. The persistence length of the backbone was altered to study the changes in radius of gyration, adsorption layer thickness, and surface occupational area.

Additionally, the influence of charge density on adsorption layer thickness and surface occupation area was studied.

Table 3.1 The summary of comb copolymer configurations implemented in Flatt et al. (2009) study.

Configuration	Structural Parameters		
	P	N	n
S1	13	3	23
S2	17	3.5	20
S3	23	3.3	25
S4	23	4.1	85
S5	23	9.25	18
S6	45	4	15
S7	45	7.4	9
S8	114	7.7	11
S9	114	14	12
S10	227	22	4

3.3 RESULTS & DISCUSSION

The summary of results comparing Flatt et al. and Wang et al. theories is provided in Table 3.2. Overall, the results are in good agreement within both models, considering that both do not provide accurate values but only estimates. Please, refer to the whole section for more concrete results.

Table 3.2 The radius of gyration of a comb copolymer in the free solution computed from Flatt et al. (2009) and Wang et al. (2018) models for several PCE configurations.

Name	Structural Parameters			R_g (nm)		ALT (nm)			S_A (nm^2)	
	P	N	n	Flatt et al.	Wang et al.	Flatt et al.	Measured*	Wang et al.	Flatt et al.	Wang et al.
S1	13	3	23	4.72	2.83	1.40	1.80	1.71	65.8	82.5
S2	17	3.5	20	4.98	3.03	1.66	1.95	1.90	76.3	89.9
S3	23	3.3	25	6.35	3.79	2.06	1.90	2.16	123.0	137.0
S4	23	4.1	85	13.82	7.69	2.02	2.40	2.16	446.3	1061.9
S5	23	9.25	18	6.41	4.52	1.86	2.65	2.16	120.6	299.8
S6	45	4	15	6.35	3.94	3.23	2.30	2.94	143.0	118.2
S7	45	7.4	9	5.29	3.57	3.04	3.40	2.93	103.2	99.8
S8	114	7.7	11	8.72	5.85	5.80	4.40	4.56	294.7	249.5
S9	114	14	12	10.36	6.91	5.47	4.40	4.56	384.6	473.6
S10	227	22	4	7.72	6.14	8.46	6.40	6.39	272.9	233.6

* The original measured values were divided by 2, since in the original study the measured values represented the distance between two particles separated by two layers of PCEs.

3.3.1 RADIUS OF GYRATION: FREE SOLUTION

Given that $l_B = 0.7$ nm, $a_N = 0.25$ nm, $\rho_e = (N - 1)/N$, $\lambda_D = 1$ nm, and $l_a = 0.37$ nm, the WLC model can be compared to the Flatt et al. model. Fig. 3.2 illustrates the radius of gyration of a single chain in dilute solution for 10 different PCE configurations.

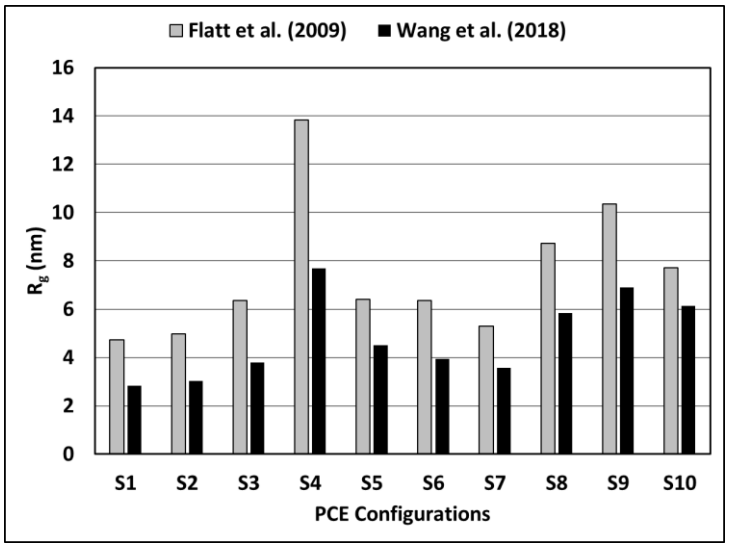

Figure 3.2 The radius of gyration computed by Flatt et al. (grey) and Wang et al. (black) theories.

According to the results, Flatt et al. model yields noticeably higher values than the model presented by Wang et al. This might be because the model by Flatt et al. does not involve the persistence length of the backbone. In contrast, Wang et al. considers the bare, electrostatic, and steric effects on the persistence length of the backbone. Despite the differences in physical background, both theories show similar trends for all presented PCE configurations.

Since PAEs have stiffer backbone than PCEs, the PAEs with the same configuration would shift towards *Stretched Backbone Worm* regime. Wang et al. model could be augmented for other regimes, such as the SBW. This is possible since the flexibility of the backbone is a variable of mean-square radius of gyration.

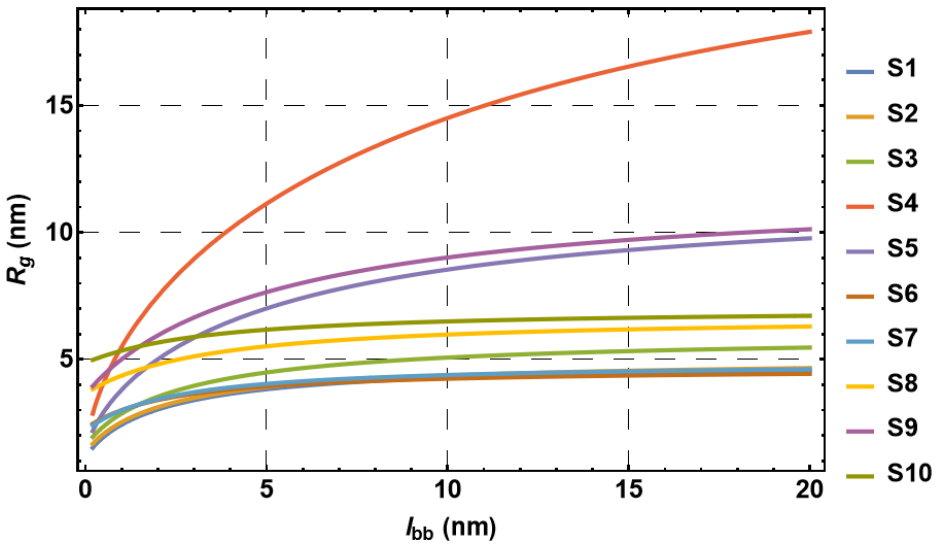

Figure 3.3 The dependence of radius of gyration on the persistence length of several PCE configurations.

Fig. 3.3 illustrates the augmentation of Wang et al. model for comb polyelectrolytes with more rigid backbones. There is a weak dependence between L_{bb} and R_g at lower persistence length values, which might be due to backbone being highly flexible that the average size of the chain is weakly affected by the backbone length. In contrast, for more rigid chains, the change in R_g is more apparent with backbone contour length because the average size approaches L_{bb}. In all cases, the radius of gyration increases with persistence length with a tendency of becoming flat at higher l_{bb} values. This is reasonable since the high rigidity of backbone resists the change of its size.

3.3.2 SURFACE OCCUPATION AREA: ADSORBED SINGLE CHAIN

The surface occupation areas of several PCE configurations in the adsorbed state were compared between Flatt et al. and Wang et al. models (Fig. 3.4). According to the results, although both theories do not coincide for certain PCE configurations (specifically for S4 and S5), overall, they have a good agreement in results, despite having different underlying physics.

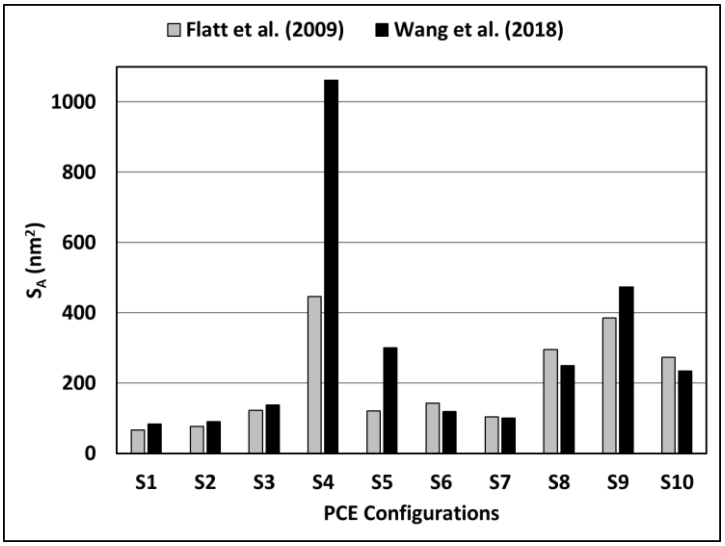

Figure 3.4 The surface occupation area computed by Flatt et al. (grey) and Wang et al. (black) theories.

Similarly, Wang et al. model could be expanded to estimate the surface occupation area of the stiffer chains in adsorbed state. The flexibility of the backbone may strongly affect the surface occupation area due to various adsorption conformations. The adsorbed chain could be fully stretched, flexible or form looped conformations. Fig. 3.5 shows the relation between S_A and l_{bb} for the given PCE configurations with various backbone rigidity predicted by Wang et al. theory for adsorbed single chains. The surface occupation area gradually increases with persistence length, until becoming flat at higher l_{bb} values. The surface occupation area of the shorter chains reaches the plateau faster compared to the

longer ones. Moreover, the longer backbone configurations (namely S4, S9, and S5) show the high surface coverage, which is consistent with the theory behind the model. As expected, more flexible backbone results in a smaller surface coverage, especially when the backbone is long, which has higher tendency to form loops. When the backbone gets shorter, its length may not be high enough to form any loops, thus, the effect of the persistence length tends to be negligible. The more rigid chains might expose larger number of anionic anchors compared to the flexible ones, wherein could potentially trap them in said loops.

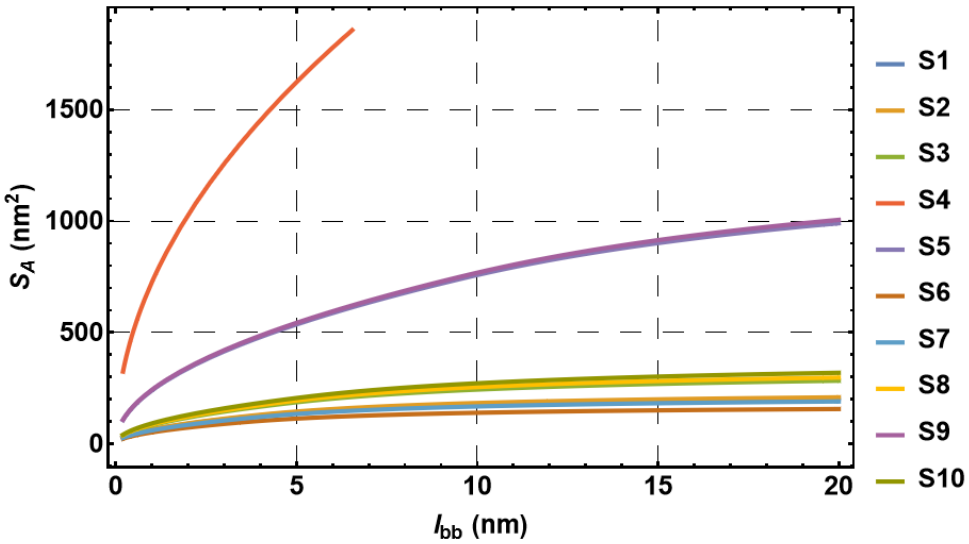

Figure 3.5 The dependence of surface occupation area on the persistence length of several PCE configurations.

In Fig. 3.6(a-c), the relation between S_A, S_A/l_{bb}, S_A/l_{bb}^2 and L_{bb}/l_{bb} is shown. The ratio indicates the transition between flexible and more rigid backbones: if the ratio is far less than 1, then the backbone is more rigid, otherwise the backbone is more flexible. According to the results, the surface occupation area reaches the plateau at low L_{bb}/l_{bb} ratio, which is in accordance with the theory (Fig. 3.6a). However, at higher ratios, S_A continuously decreases without reaching the plateau. Nonetheless, the practical range for the ratio would be in the order of magnitude of ~100, up to which the model can be reliable. In Fig. 3.6b, the S_A/l_{bb} ratio increases with L_{bb}/l_{bb} and the transition from semi-flexible to flexible occurs at approximately L_{bb}/l_{bb} ~ 1-2. The longer chains exhibit higher S_A/l_{bb} values as expected from the model. Fig. 3.6c demonstrates the dimensionless plot of Fig. 3.6(a-b). All configurations lie on a single curve, indicating the flexibility of WLC model for various comb copolymer configurations.

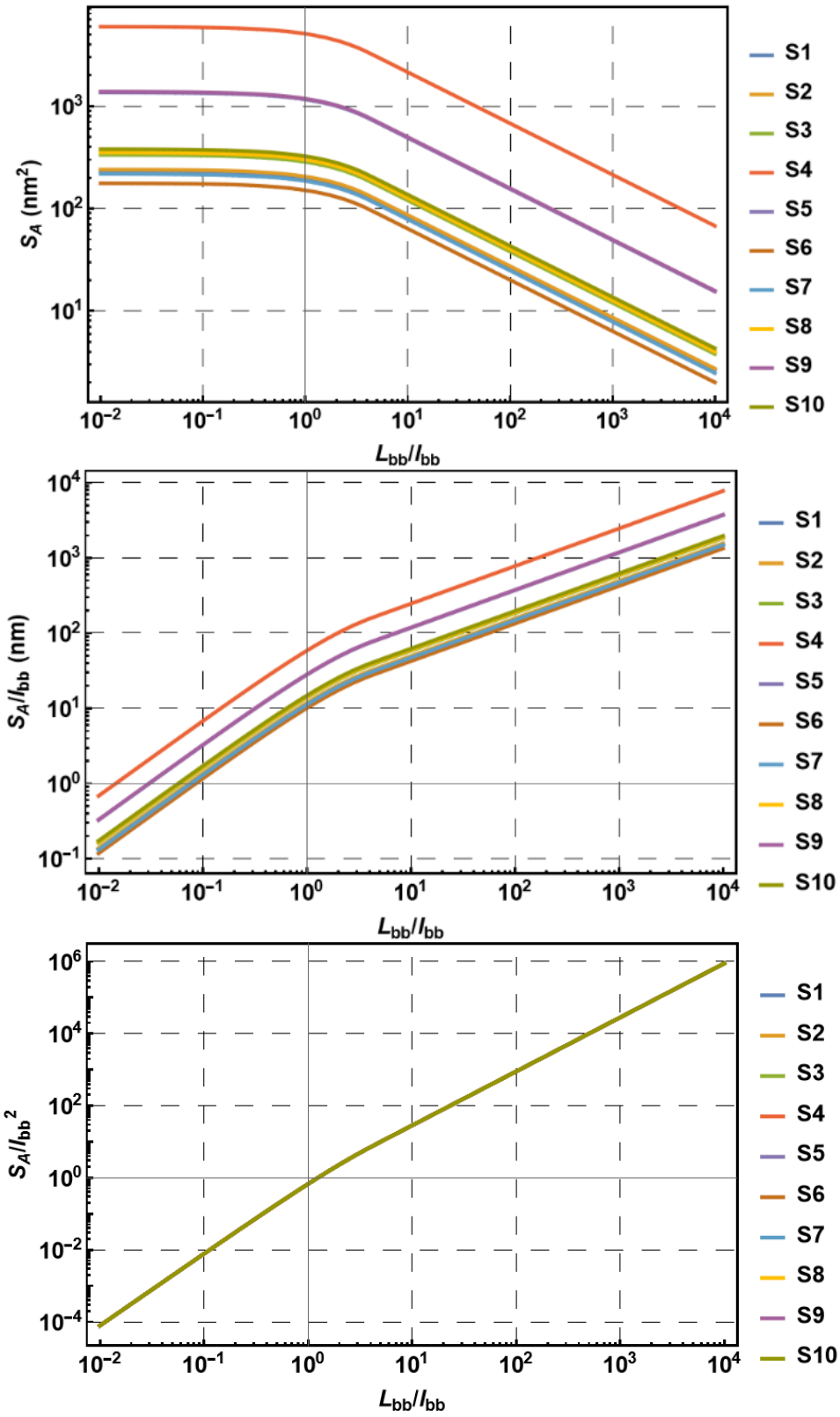

Figure 3.6 The dependence of (a) S_A, (b) S_A/l_{bb} and (c) S_A/l_{bb}^2 on L_{bb}/l_{bb} of several PCE configurations.

Fig. 3.7 demonstrates how log(S_A) changes with the number of backbones repeating units and the backbone charge density. The results show that surface occupation area increases with n and ρ_e, supporting the previous findings. The higher charge density means

stronger electrostatic interaction between the backbone and the charged surface, thus reducing the possibility of backbone detachment from the surface.

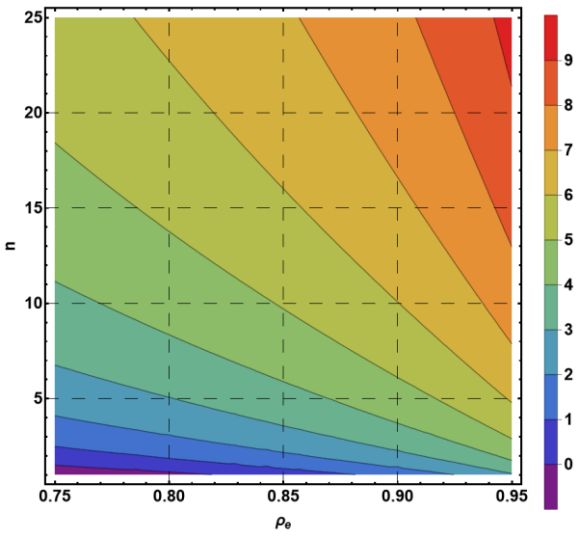

Figure 3.7 The contour plot of log(S_A) versus number of repeating units (n) and charge density (ρ_e).

3.3.3 ADSORPTION LAYER THICKNESS: ADSORBED SINGLE CHAIN

Fig. 3.8 summarizes the layer thicknesses in accordance with Flatt et al. and Wang et al. theories. According to the results, both theories predicted approximately the same layer thickness, especially for low ALT, whereas there are some fluctuations for higher ALT values. Despite being different in physical nature, both theories show similar results.

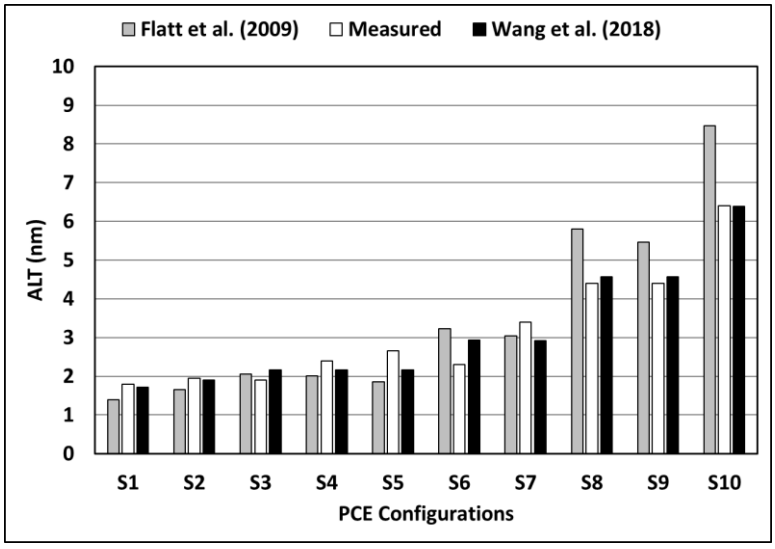

Figure 3.8 The adsorption layer thickness (ALT) computed by Flatt et al. (grey) and Wang et al. (black) theories, compared to experimental results (white) provided by Flatt et al. (2009).

When augmenting Wang et al. theory to the more rigid backbones, the results showed a certain transition (Fig. 3.9). The initial curves suddenly became discontinuous

and became horizontal lines. This might indicate the transition between fully adsorbed and partially adsorbed states. When the flexibility of the backbone is high, the entrapment of anionic anchors may cause weak adsorption, which leads to regions with higher ALT. However, as the rigidity of backbone increases, the more negative charges are exposed, resulting in stronger adsorption. The adsorption layer thickness of fully adsorbed comb copolymers will depend on the sidechain conformation, either mushroom or brush-like. The transition points are different for each PCE configuration. However, the changes of conformation are similar.

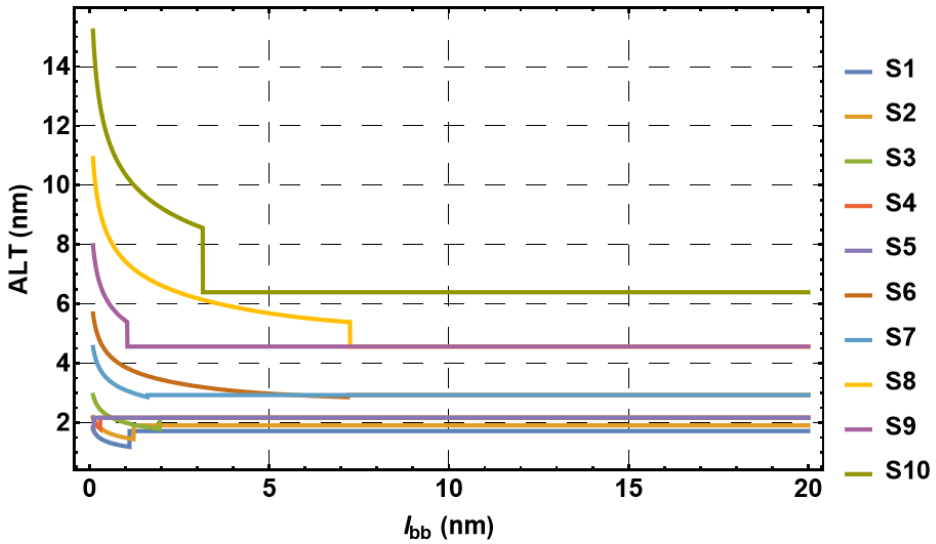

Figure 3.9 The dependence of adsorption layer thickness on persistence length of backbone of several PCE configurations.

Fig. 3.10 demonstrates how adsorption thickness layer changes with the number of sidechain monomers and the backbone charge density. The results possibly show the transition between brush and mushroom regimes. At lower charge density, the grafting density is higher, thus the ALT becomes higher because of a stretch of sidechains. On the other hand, the higher charge density results in lower grafting density, which ultimately leads to mushroom conformation of sidechains. In this state, the ALT becomes lower, since the sidechains are coiled a little, resembling mushroom heads. In this state, the adsorption layer thickness strongly depends on the sidechain conformation. Additionally, the ALT increases with P in both regimes, as sidechains length predominantly determines the adsorption layer thickness.

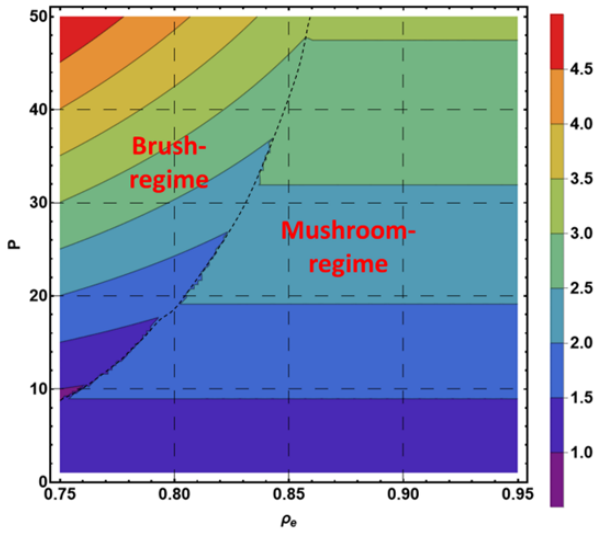

Figure 3.10 The contour plot of ALT versus number of sidechain monomers (P) and charge density (ρ_e).

3.4 CONCLUSION

In general, the following conclusions can be made:

- Both Flatt et al. and Wang et al. theories can be applied to FBW regime.
- Both theories have good agreement in results, even though the physical background is different.
- Wang et al. theory could be extended for comb copolymers with more rigid backbones.
- Flatt et al. theory does not consider the backbone flexibility but rather focuses on the Helmholtz free energy minimization and the scaling theory, therefore its application for PAEs is limited.
- According to Wang et al. theory, the persistence length of the backbone affects the conformation of comb copolymers in both free solution and adsorbed single chain states: R_g and S_A increased with l_{bb}; depending on the comb configuration, the change in conformation was more noticeable, especially for those having longer backbone (R_g and S_A) and longer sidechains (ALT); ALT reduced with l_{bb} in partially adsorbed state, whereas was constant in fully adsorbed state, in which ALT only depends on sidechain conformation; the transition between both regimes was discontinuous.
- Grafting density determines the transition between brush and mushroom conformations: at higher backbone charge density (lower grafting density), the adsorption layer thickness was constant; as the charge density reduced (higher grafting density), the ALT started to rise at certain point; the transition was discontinuous.

CHAPTER 4 – MOLECULAR DYNAMICS SIMULATIONS

4.1 INTRODUCTION

In this chapter, the coarse-grained molecular dynamics simulations were performed to study the influence of backbone flexibility on the comb copolymer conformations in free solution and adsorbed single chain states.

4.2 METHODOLOGY

4.2.1 CONFORMATIONAL PROPERTIES IN FREE SOLUTION

To observe the effect of persistence length, the number of backbone monomers and the number of sidechain monomers on the conformation of a single chain comb-like polyelectrolyte copolymer in a free solution, the coarse-grained molecular dynamics simulations were performed on the open-source LAMMPS software. Three chain configurations were modeled. The summary of copolymer structural parameters is given in Table 4.1. The simulation snapshots of initial system configuration can be seen on Fig. 4.1. The simulation system of 200x200x200 (LJ units) consisted of polyelectrolyte chain and counterions. The number of counterions was calculated as the number of charged units in backbone:

$$N_{ions} = (N - 1) \times n \qquad \text{Eq. 4.1}$$

Although the inclusion of water molecules would accurately represent the polyelectrolyte solution, the cost of simulation becomes significantly high. Therefore, instead of explicit solvent, the implicit solvent approach was adapted. In this case, the random bombardment by water molecules was simulated by the Langevin thermostat in NVT ensemble and the dielectric constant of water was set as 0.51.

Table 4.1 The structural parameters and number of counterions of three comb copolymer configurations.

Configuration	Structural Parameters			Counterions
	P	N	n	
CP1	23	7	15	90
CP2	30	7	15	90
CP3	23	3	15	30

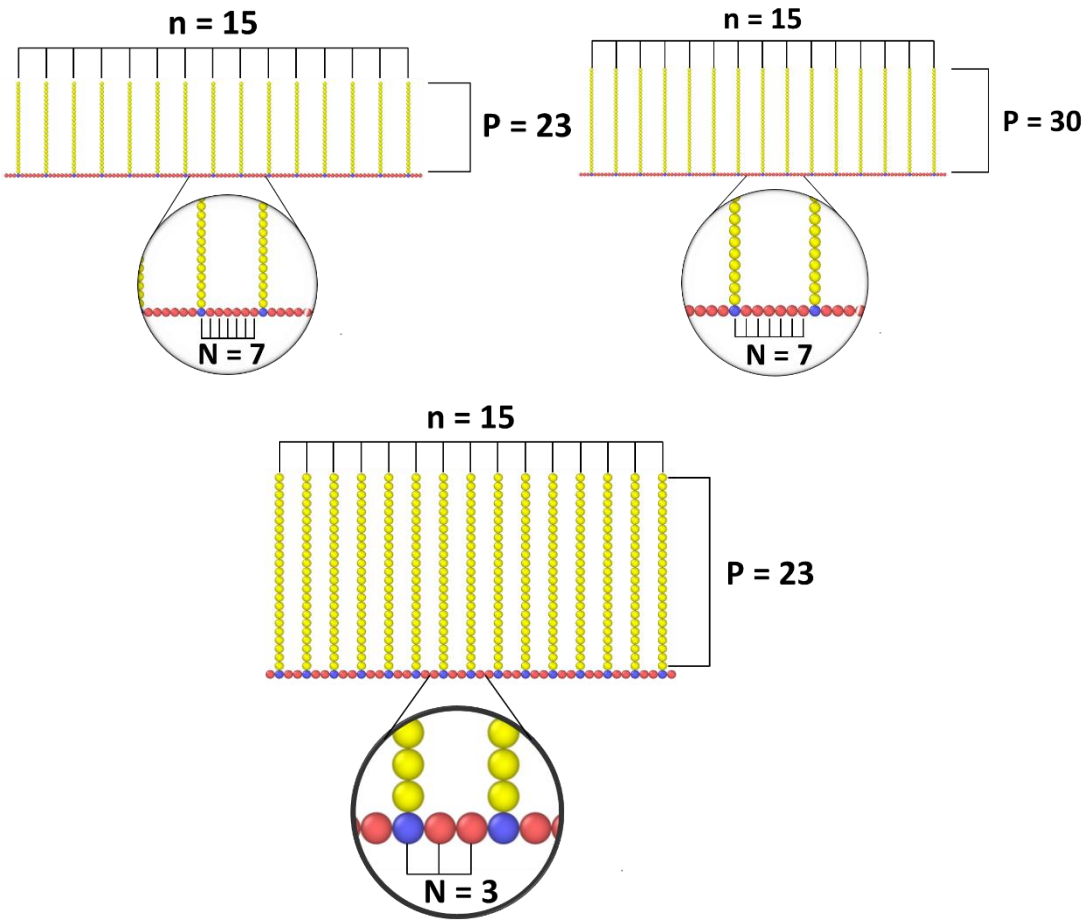

Figure 4.1 Comb configurations of CP1 (top left), CP2 (top right), and CP3 (bottom).

The simulation system had periodic boundaries in all dimensions. All bonds were set as harmonic. The harmonic bond potential has the following form:

$$V_{bond} = K_{bond}(r - r_0)^2 \qquad \text{Eq. 4.2}$$

where V_{bond} = the potential energy of the bond, K_{bond} = the bond coefficient, r = the distance between bonded particles and r_0 = the equilibrium bond distance. There were 2 bond types: those that connected particles in the backbone and those between sidechain monomers, including the bonds that connected sidechains to the backbone. The bond coefficients were set as 15.0 and 10.0 in LJ units, respectively. The equilibrium bond distances were set as 1.0 and 1.5 in LJ units, respectively. The angles between bonds were modeled using the cosine potential, which has the following expression:

$$V_\theta = K_\theta[1 + \cos(\theta)] \qquad \text{Eq. 4.3}$$

where V_θ = the potential energy of bending, K_θ = the angle coefficient and θ = the angle between adjacent bonds. There were two angle types used: the angles between two adjacent backbone bonds and the angles between two adjacent sidechain bonds, including the angles

between adjacent sidechain and backbone bonds. The angle coefficient for the sidechains was set as 1.0 in LJ units and for the backbone was set as a variable.

The interactions between particles were described by Lennard-Jones and Coulomb potentials. The Lennard Jones potential describes the interaction between non-bonded particles and has the following form:

$$V_{LJ} = \begin{cases} 4\varepsilon_{LJ}\left[\left(\frac{\sigma}{r}\right)^{12} - \left(\frac{\sigma}{r}\right)^{6}\right] & r \le r_c \\ 0 & r > r_c \end{cases} \quad \text{Eq. 4.4}$$

where V_{LJ} = the LJ potential, r = the distance between paired particles, r_c = the cutoff distance, ε = the well depth and σ = the particle size. The cutoff distance was set as 1.12 in LJ units. The Coulomb potential describes the interaction between charged particles:

$$V_{Coul}(r) = \frac{q_i q_j}{4\pi\epsilon_0 r_{ij}} \quad r < r_c \quad \text{Eq. 4.5}$$

where V_{Coul} = the Coulomb potential, q_i, q_j = the particle charges, r_{ij} = the distance between particles i and j, r_c = the cutoff distance and ϵ_0 = the vacuum permittivity. The cutoff distance for the Coulomb interaction was set as 5.0 in LJ units.

The cosine potential defines how likely the chain is to bend. Thus, it can be used to describe the persistence length of the backbone that is determined by the angle coefficient *K*. The simulations were performed for K in range of 2-30 in LJ units, where low values corresponded to flexible chain and higher values to rigid chains. In total, 135 simulations were performed, 3 simulations for each K value for each of 3 configurations. Different random number seeds were set for each simulation. The simulation run was set to $2x10^7$ timesteps with the timestep of 0.005 in LJ units. The simulation snapshots were created by OVITO Basic VMD software.

The radius of gyration was computed as follows:

$$R_g^2 = \frac{1}{N}\sum_{k=1}^{N} |\boldsymbol{r}_k - \boldsymbol{r}_{mean}|^2 \quad \text{Eq. 4.6}$$

where R_g = the radius of gyration, $\mathbf{r}_k$ = the position vector of particle k, $\mathbf{r}_{mean}$ = the mean position vector of all particles and N = the number of particles.

4.2.2 CONFORMATIONAL PROPERTIES IN ADSORBED STATE

To examine the influence of persistence length on the conformation of a single chain comb-like polyelectrolyte copolymer in an adsorbed state, coarse-grained molecular dynamics simulations were performed on the open-source LAMMPS software. The chain structural parameters of combs were as described in Table 4.1. The simulation system of similar size consisted of the polyelectrolyte chain, the charged surface and counterions. The number of counterions was calculated as the number of charged units in backbone plus the charges on the surface:

$$N_{ions} = (N-1) \times n + Z \times q \qquad \text{Eq. 4.7}$$

where Z = the valence of charged particles on the surface and q = the number of charged particles on the surface.

To simulate the charged surface, 1521 charged particles were uniformly placed on xy-plane, each having +2 charge. The number of counterions for each copolymer configuration is provided in Table 4.2.

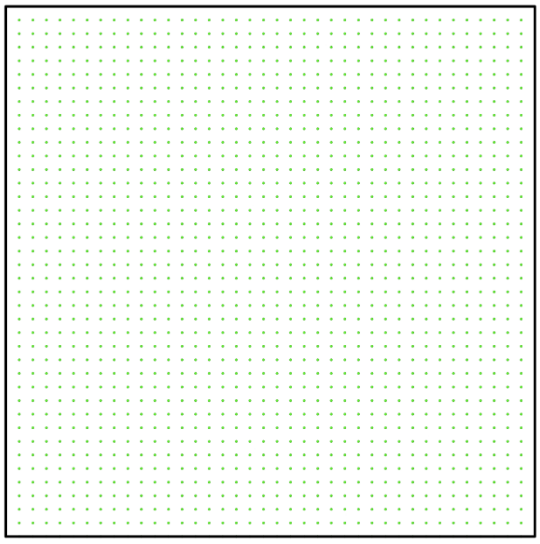

Figure 4.2 The simulation snapshot of charged surface.

Table 4.2 The structural parameters and number of counterions of three comb copolymer configurations.

Configuration	Counterions
CP1	3132
CP2	3132
CP3	3072

The implicit solvent approach was applied to reduce the computational cost. The simulation system had periodic boundaries in x and y directions. In z direction, the boundaries were non-periodic to simulate the charged surface. The bonds and the angles were simulated as same as in Section 4.2.1.

The adsorption simulations were divided into two parts. In the first part, the interactions between copolymer chain and the surface were disabled to simulate the relaxation of the chain in free solution. The second part is the continuation of the relaxation, where the final conformation of the relaxation is taken as the initial conformation to simulate the adsorption process. The cutoff distances for the Lennard-Jones and Coulomb potentials were set as same as in Section 4.2.1 for the relaxation part. For the second part, the Lennard-Jones cutoff was set as 1.12 in LJ units and the Coulomb cutoff was set to be 20.0 in LJ units. The higher cutoff is because the chain must interact with the surface to initiate the adsorption. In both parts, the surface charges were fixed on the x-y plane with *fix setforce* command, whereas the mobile particles were kept between two parallel planes using *fix wall/lj126* command.

The cutoff distance can be used for Lennard Jones interaction, since the potential reaches zero at relatively short distances. However, electrostatic interaction is referred to as long-range interaction, where the presence of forces cannot be neglected at long distances. This increases the cost of computation because every pairwise interaction must be accounted for. However, this can be avoided by implementing the Ewald method, particularly Particle-Particle Particle-Mesh (PPPM) method, which interpolates the charges into a grid, which allows the computation of discrete Poisson's equation to be handled in Fourier's plane.

The simulations were performed for K in range of 2-30 in LJ units, where low values corresponded to flexible chain and higher values to rigid chains. For each comb configuration, 90 simulations were performed (45 for relaxation and 45 for adsorption parts), which is the total of 270 simulations. Different random number seeds were set for each simulation. The simulation run for the relaxation was set to be 20×10^7 timesteps and for the adsorption part to 10^6 timesteps with the timestep of 0.005 in LJ units. The simulation snapshots were created by OVITO Basic VMD software. The radius of gyration was computed as in Eq. 4.6. The adsorption layer thickness and surface occupation area were calculated as in Eq. 2.2 and Eq. 2.4, respectively.

4.3 RESULTS & DISCUSSION

4.3.1 CONFORMATIONAL PROPERTIES IN FREE SOLUTION

Fig. 4.3(a-b) illustrate the evolution of average radius of gyration of CP1 configuration with simulation time in linear and logarithmic scale for K = 2.0, respectively, from 3 sets of simulations. The identification of the mean radius of gyration from the linear scale graph was inconvenient since it was not apparent when the system reached the equilibrium state. Therefore, it was more convenient to refer to the logarithmic time scale, where the equilibration state was more apparent and could be neglected. The equilibrium state was reached in approximately $2x10^6$ timesteps. The evolution of radius of gyration for other simulations can be seen in Appendix A.

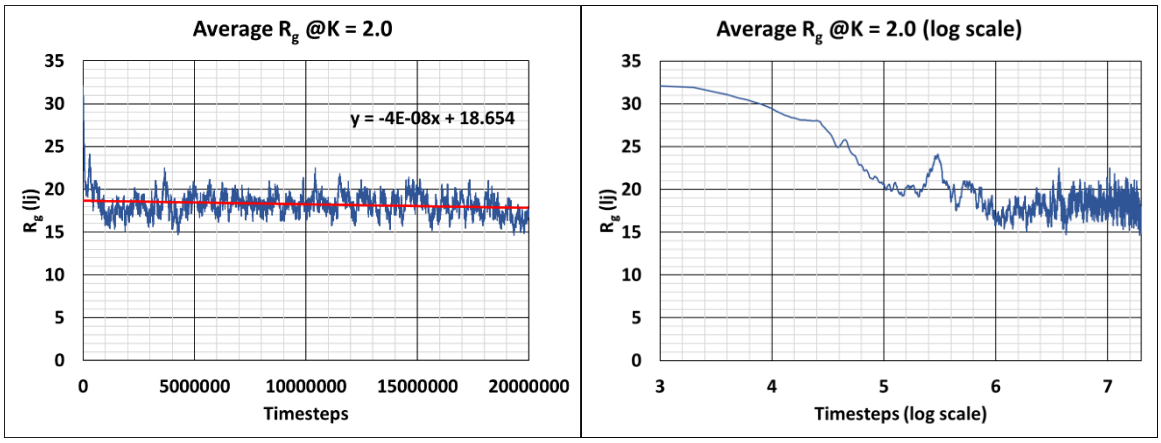

Figure 4.3 The average radius of gyration of CP1 as a function of time for K = 2.0 (a) linear and (b) logarithmic scale.

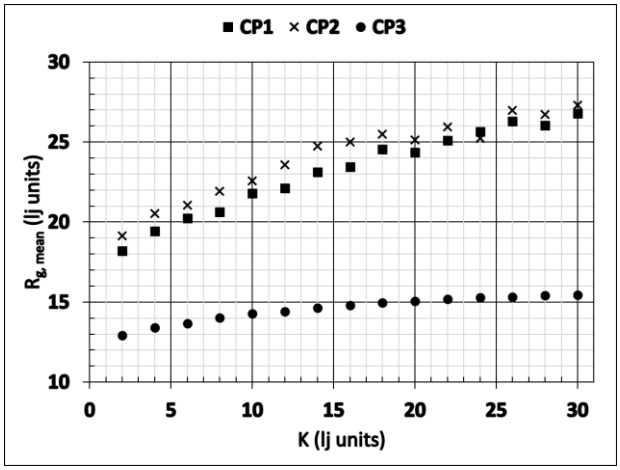

Figure 4.4 The mean radius of gyration as a function of angle coefficient K in Lennard-Jones units for configurations CP1, CP2, and CP3 in free solution.

Fig. 4.4 illustrates the mean radius of gyration of CP1, CP2, and CP3 configurations in free solution with various chain flexibilities. According to the results, the radius of

gyration gradually increases with the bending stiffness of the backbone. The configuration with the shortest backbone (CP3) exhibited the most consistent results. On the other hand, the configuration with the longest sidechains (CP2) had some fluctuations, especially at higher K values. This might be due to longer sidechains, as the effect of sidechain length becomes more prevalent on R_g. The CP1 configuration, being as the intermediate between CP2 and CP3 configurations, had minor fluctuations at higher K values, but attained a similar trend as the other two. According to the most consistent data, the curve seems to be reaching the plateau, indicating that at arbitrarily higher K, the effect of the backbone rigidity would be negligible and R_g would only be a function of n, N, and P. In general, copolymers with lower N had smaller R_g compared to others, whereas those with higher P were bigger. Overall, the results are consistent with the polymer physics theories.

4.3.2 CONFORMATIONAL PROPERTIES IN ADSORBED STATE

To evaluate the conformational properties (ALT and S_A) of comb copolymers in the adsorbed state, Flatt et al. theory was used. Moreover, the average radius of gyration had to be calculated for the copolymers in adsorbed state, excluding the simulation steps where the backbone had not been adsorbed yet. This was done by manually observing the simulation snapshots using OVITO Basic VMD software. The averaging was done after the complete adsorption of the backbone on the charged surface. It should be noted that this might not show accurate results, since the copolymer requires some time to equilibrate on the surface.

Fig. 4.5 shows the mean radius of gyration of CP1, CP2, and CP3 configurations in the adsorbed state with different chain flexibility. According to the results, the data fluctuated for all configurations, so the possible plateau region was not identified. Nevertheless, the trends were similar. The mean radius of gyration slightly increased with K. The adsorbed state radius of gyration was lower for the configuration with lower N, similar to the radius of gyration in free solution. However, the difference between higher and lower P was not as apparent. Overall, the results coincided with theoretical models.

Comparing Fig. 4.4 and Fig. 4.5, the radius of gyration of comb copolymer in adsorbed state is slightly higher than in free solution state. This could be due to backbone movement in z direction being hindered by surface, which led to its partial stretch.

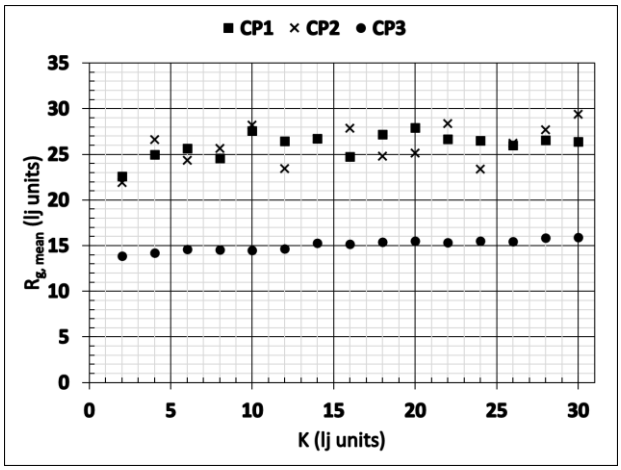

Figure 4.5 The mean radius of gyration as a function of angle coefficient K in Lennard Jones units for configurations CP1, CP2, and CP3 in adsorbed state.

Fig. 4.6 depicts the mean adsorption layer thickness of CP1, CP2, and CP3 configurations in the adsorbed state with various K. According to the results, the mean adsorption layer thickness only slightly increased as the backbone became more rigid. This is because the ALT values were calculated at full adsorption, where according to theory, ALT does not depend on backbone flexibility. Interestingly, the ALT was lower for the configuration with lower N, although the number of sidechains and sidechain monomers were practically the same. This might be due to high grafting density that resulted in steric hindrance between adjacent sidechains, which could lead to their repulsion from each other. From the figure, it was difficult to observe, but the ALT was slightly higher for configuration with higher P. The difference in ALT between those two configurations is quite small, but it is justified by the small difference in P. Overall, the results coincided with theory.

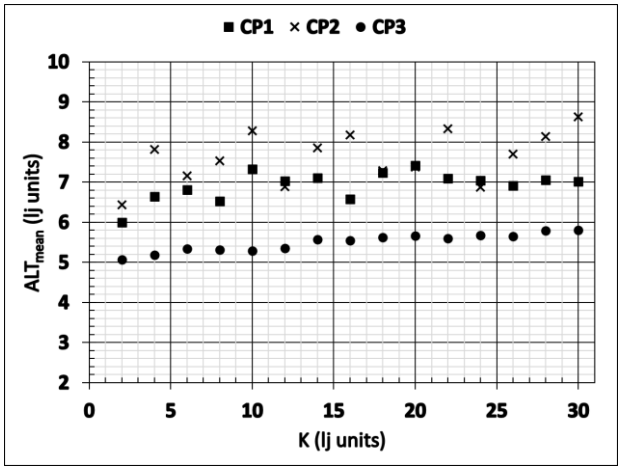

Figure 4.6 The adsorbed layer thickness as a function of angle coefficient K in Lennard-Jones units for configurations CP1, CP2, and CP3 in adsorbed state.

Fig. 4.7 illustrates how the mean surface occupation area of CP1, CP2, and CP3 configurations in the adsorbed state changed with K. According to the results, the data fluctuated for all configurations, so the possible plateau region could not be determined, as well, same as in previous findings. Nonetheless, the trends were similar for all configurations. The mean surface occupation area only slightly increased with the bending stiffness. Moreover, $S_{A,mean}$ was lower for the configuration with lower N. It was quite difficult to determine which configuration exhibited higher S_A between CP1 and CP2, since their structures were almost similar, but the one with lower N had lower surface coverage. This was due to a shorter backbone. Overall, the results coincided with theoretical models.

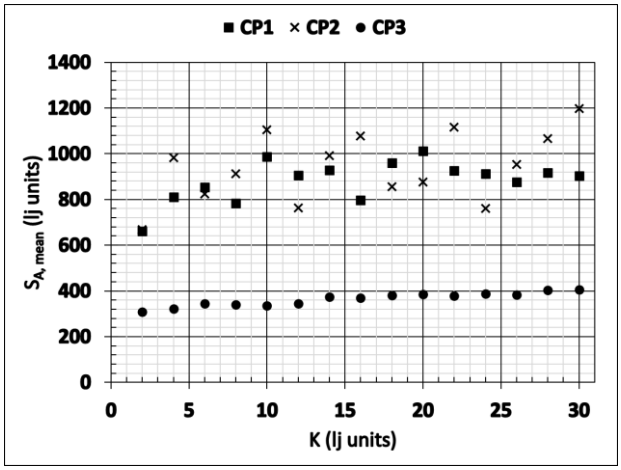

Figure 4.7 The surface occupation area as a function of angle coefficient K in Lennard-Jones units for configurations CP1, CP2, and CP3 in adsorbed state.

4.3.3 SIMULATION SNAPSHOTS

Observing the simulation snapshots revealed some interesting results. The time for the comb copolymer to adsorb to the surface from its free solution state depended on the backbone charge density. One simulation ended up with copolymer not being adsorbed at all. Fig. 4.8 shows the initial and final conformations of the non-adsorbed chain. The chain initially had the random conformation. However, at the final timestep, the backbone seems to be oriented in parallel to the surface. Moreover, the distance between the surface and the copolymer is lower at the end of the simulation, which implies the attractive interaction between backbone and surface. Possibly, the system was too big, or the duration of simulation was too short for the complete adsorption to occur.

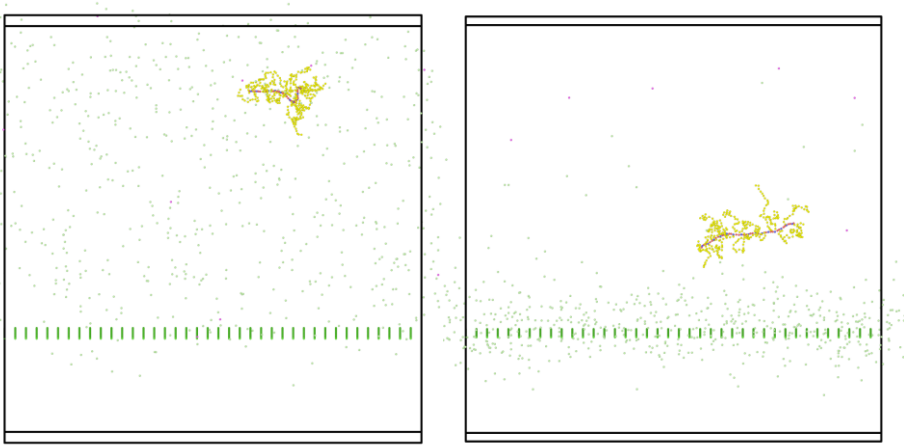

Figure 4.8 The initial (left) and final (right) conformations of non-adsorbed chain.

Moreover, the snapshots depicted a formation of loops for some copolymers with longer backbones (Fig. 4.9). Such observations were not made for configuration with shorter backbone. However, generally the final conformations were without loops. The more flexible combs had unstretched backbones. As the backbone stiffness increased, the backbones became more stretched. Interestingly, some combs had fully stretched backbones even at moderate stiffnesses (refer to Fig. 4.10). See Appendix B for more simulation snapshots.

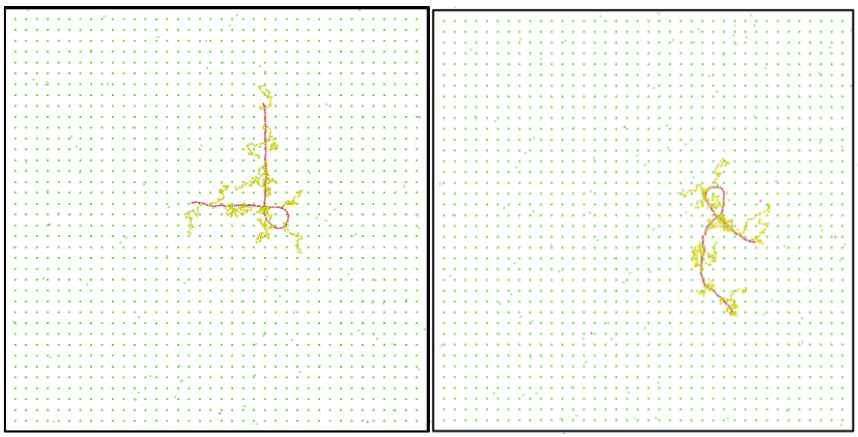

Figure 4.9 The loop conformations in adsorbed state.

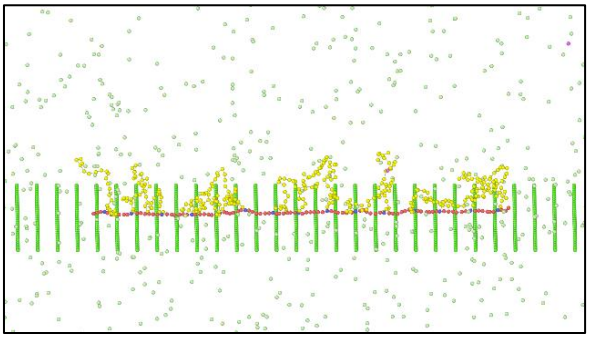

Figure 4.10 The final conformation of CP1 with K = 12.0.

4.4 CONCLUSION

The results of this chapter lead to the following conclusions:

- R_g of comb in free solution increased with higher backbone rigidity: at higher K values, the mean radius of gyration reached the plateau region, coinciding with theory;
- In free solution, the radius of gyration increases with N and P;
- R_g of comb in adsorbed state also increased with the stiffness of the backbone, ultimately reaching the plateau region at high K;
- R_g of comb in adsorbed state was slightly higher than in free solution state: the surface hinders free movement of backbone, leading to slight stretch of backbone;
- ALT seemingly did not change due to backbone flexibility: the ALT was calculated for the chains after they were fully adsorbed, where the backbone flexibility has no effect on the ALT;
- ALT was slightly higher when P slightly increased, whereas it was lower for smaller N: smaller N implies higher grafting density, at which the adjacent sidechains could repel each other due to steric hindrance, which reduces ALT;
- S_A slightly increased with backbone stiffness: the more stretched backbone exposes more anchors for adsorption, thus covering more surface;
- S_A increases with N, while does not depend on P, as expected from the theory;
- Combs with smaller backbone charge density (smaller N) took longer time to adsorb, with one not adsorbing at all: higher charge density implies stronger attractive interaction between comb copolymer backbone and charged surface, which leads to faster and stronger adsorption.
- Copolymers with long backbones may form loop conformations.

CHAPTER 5 – SUMMARY AND FUTURE RESEARCH

PAEs have a potential to be a new state-of-the-art superplasticizer due to enhanced performance in cement pastes. The better workability and rheology of cement and PAEs higher tolerance to clay content shows promising future for the concrete admixture industry. However, a significant fraction of research has been done on the experimental part only. Currently, it requires the extensive computational studies to identify the effect of aromacity of backbone, backbone flexibility, and anionic anchors on the adsorption of PAEs on the cement surface and conformation of PAEs in adsorbed state.

In this research, the effect of the flexibility of comb copolymer polyelectrolyte on its conformations in free solution and adsorbed single chain states was studied using existing polymer physics theories and the coarse-grained molecular dynamics simulations. The results imply that it is quite possible to use coarse-grained MD simulations coupled with Gay and Raphael's (2001) structural model to describe the conformational properties of PAEs, referring to the existing studies on PCEs. The results from theoretical equations revealed that both Flatt et al. (2009) and Wang et al. (2018) theories can be applied to comb copolymers in *FWB* regime. The two theories coincided with experimental results, despite having different theoretical backgrounds. Flatt et al. did not consider the flexibility of the backbone in their theory, which is why it cannot be implemented for copolymers with more rigid backbones in *SBW* regime. However, Wang et al. theory can potentially be implemented to describe the conformations of such copolymers.

In general, the analytical results and simulation results showed similar trends for mean radius of gyration in free solution and adsorbed single chain states, along with the surface occupation area and adsorption layer thickness. In the case of the latter, the backbone flexibility had no visible effect on the ALT due to backbones being completely adsorbed. This demands further investigation to determine the effect of backbone flexibility in case of weak adsorption.

Additionally, observations of simulation snapshots revealed the dependance of backbone charge density on the adsorption. Those backbones with smaller charge density had weaker interactions with the surface, which led to increased adsorption time. Some copolymers formed looped conformations. This is possible because there were only single chains on the surface. In case of multiple chains, the copolymers would be densely packed.

However, for future research it is suggested to greatly increase the bending modulus (K_θ) of the backbone to see how the results might change. Moreover, the all-atom MD simulations are required to obtain more accurate data on the influence of aromacity, backbone flexibility and various anionic functional groups on PAE's adsorption behavior.

BIBLIOGRAPHY

[1] Breilly, D., Fadlallah, S., Froidevaux, V., Colas, A., & Allais, F. (2021). Origin and industrial applications of lignosulfonates with a focus on their use as superplasticizers in concrete. *Construction and Building Materials*, *301*, 124065. https://doi.org/10.1016/j.conbuildmat.2021.124065

[2] Ramachandran, V. S., & Malhotra, V. M. (1995). Superplasticizers. In *Concrete Admixtures Handbook: Properties, Science, and Technology* (pp. 410–411). essay, Noyes Publications.

[3] Ma, Y., Bai, J., Shi, C., Sha, S., & Zhou, B. (2021). Effect of pces with different structures on hydration and properties of cementitious materials with low water-to-binder ratio. *Cement and Concrete Research*, *142*. https://doi.org/10.1016/j.cemconres.2020.106343

[4] Khudhair, M. H. R., Hilal, B. E., & Elharfi, A. (2018). Review on chemical (organic) admixtures in the cementitious materials. *Journal of Materials and Environmental Sciences*, *9*(6), 1722–1734. https://doi.org/10.26872/jmes.2018.9.6.192

[5] Gelardi, G., Mantellato, S., Marchon, D., Palacios, M., Eberhardt, A. B., & Flatt, R. J. (2016). Chemistry of chemical admixtures. *Science and Technology of Concrete Admixtures*, 149–218. https://doi.org/10.1016/b978-0-08-100693-1.00009-6

[6] National Academies Press. (2014). *Review of the formaldehyde assessment in the National Toxicology Program 12th report on Carcinogens*.

[7] Sosa, M. E., Villagrán Zaccardi, Y. A., Peralta, J. P., & Zega, C. J. (2018). Efficiency of cement-admixture systems in mortars with binary and ternary Portland cements. *DYNA*, *85*(204), 134–142. https://doi.org/10.15446/dyna.v85n204.66468

[8] Chuang, P.-H., Tseng, Y.-H., Fang, Y., Gui, M., Ma, X., & Luo, J. (2019). Effect of side chain length on polycarboxylate superplasticizer in aqueous solution: A computational study. *Polymers*, *11*(2), 346. https://doi.org/10.3390/polym11020346

[9] Li, S., Liu, J., Yang, Y., Qi, S., Ran, Q., & Liu, J. (2019). Synthesis, performance and working mechanism of a novel polyaryl ether superplasticizer for cement-based materials. *Journal of Dispersion Science and Technology*, *41*(1), 1–10. https://doi.org/10.1080/01932691.2018.1461638

[10] Sha, S., Wang, M., Shi, C., & Xiao, Y. (2020). Influence of the structures of polycarboxylate superplasticizer on its performance in cement-based materials-A Review. *Construction and Building Materials*, *233*, 117257. https://doi.org/10.1016/j.conbuildmat.2019.117257

[11] Shu, X., Ran, Q., Liu, J., Zhao, H., Zhang, Q., Wang, X., Yang, Y., & Liu, J. (2016). Tailoring the solution conformation of polycarboxylate superplasticizer toward the improvement of dispersing performance in cement paste. *Construction and Building Materials*, *116*, 289–298. https://doi.org/10.1016/j.conbuildmat.2016.04.127

[12] Kraus, A., Mazanec, O., Dengler, J., Hillesheim, N., & Bokern, J. (2014). (rep.). *Influence of PAE, SMD and PCE superplasticizers on the rheological properties of mortars and concretes*. Retrieved November 19, 2022, from https://www.rilem.net/images/publis/16848fe896809b7494c29b80f42ff4e4.pdf.

[13] Lei, L., & Plank, J. (2012). Synthesis, working mechanism and effectiveness of a novel cycloaliphatic superplasticizer for concrete. *Cement and Concrete Research*, *42*(1), 118–123. https://doi.org/10.1016/j.cemconres.2011.09.003

[14] Ng, S., & Plank, J. (2012). Interaction mechanisms between na montmorillonite clay and MPEG-based polycarboxylate superplasticizers. *Cement and Concrete Research*, *42*(6), 847–854. https://doi.org/10.1016/j.cemconres.2012.03.005

[15] Liu, X., Guan, J., Lai, G., Wang, Z., Zhu, J., Cui, S., Lan, M., & Li, H. (2017). Performances and working mechanism of a novel polycarboxylate superplasticizer synthesized through changing molecular topological structure. *Journal of Colloid and Interface Science*, *504*, 12–24. https://doi.org/10.1016/j.jcis.2017.05.025

[16] Gay, C., & Raphaël, E. (2001). Comb-like polymers inside nanoscale pores. *Advances in Colloid and Interface Science*, *94*(1-3), 229–236. https://doi.org/10.1016/s0001-8686(01)00062-8

[17] Flatt, R. J., Schober, I., Raphael, E., Plassard, C., & Lesniewska, E. (2009). Conformation of adsorbed comb copolymer dispersants. *Langmuir*, *25*(2), 845–855. https://doi.org/10.1021/la801410e

[18] Wang, Y., Shu, X., Yang, Y., Ran, Q., & Liu, J. (2018, January). Polymer physics and PCE superplasticizers revisited. In 12th International Conference on Superplasticizers and other Chemical Admixtures in Concrete, ICSP 2018.

[19] Rüttgers, A., & Griebel, M. (2018). Multiscale simulation of polymeric fluids using the sparse grid combination technique. *Applied Mathematics and Computation*, *319*, 425–443. https://doi.org/10.1016/j.amc.2017.04.025

[20] Zhao, H., Yang, Y., Song, S., Shu, X., Chen, W., Jin, W., & Ran, Q. (2020). Adsorption conformation of comb-shaped polycarboxylate ethers on Ettringite (100) surface: An atomic scales simulation. *Journal of Computational Biophysics and Chemistry*, *20*(01), 99–108. https://doi.org/10.1142/s2737416521500071

[21] Shu, X., Zhao, H., Wang, X., Zhang, Q., Yang, Y., Ran, Q., & Liu, J. (2016). Effect of hydrophobic units of polycarboxylate superplasticizer on the flow behavior of cement paste. *Journal of Dispersion Science and Technology*, *38*(2), 256–264. https://doi.org/10.1080/01932691.2016.1160831

[22] Javadi, A., Jamil, T., Abouzari-Lotf, E., Soucek, M. D., & Heinz, H. (2021). Working mechanisms and design principles of comb-like polycarboxylate ether superplasticizers in cement hydration: Quantitative insights for a series of well-defined copolymers. *ACS Sustainable Chemistry & Engineering*, *9*(25), 8354–8371. https://doi.org/10.1021/acssuschemeng.0c08566

[23] Zhang, Q., Ran, Q., Zhao, H., Shu, X., Yang, Y., Zhou, H., & Liu, J. (2016). PH-induced conformational changes of comb-like polycarboxylate investigated by experiment and Simulation. *Colloid and Polymer Science*, *294*(11), 1705–1715. https://doi.org/10.1007/s00396-016-3932-5

[24] Hirata, T., Branicio, P., Ye, J., Zheng, J., Tomike, Y., Lange, A., Plank, J., & Sullivan, M. (2017). Atomistic dynamics simulation to solve conformation of model PCE superplasticisers in water and cement pore solution. *Advances in Cement Research*, *29*(10), 418–428. https://doi.org/10.1680/jadcr.16.00137

[25] Hirata, T., Ye, J., Branicio, P., Zheng, J., Lange, A., Plank, J., & Sullivan, M. (2017). Adsorbed conformations of PCE superplasticizers in cement pore solution unraveled by molecular dynamics simulations. *Scientific Reports*, *7*(1). https://doi.org/10.1038/s41598-017-16048-3

[26] Jamil, T., Javadi, A., & Heinz, H. (2020). Mechanism of molecular interaction of acrylate-polyethylene glycol acrylate copolymers with calcium silicate hydrate surfaces. *Green Chemistry*, *22*(5), 1577–1593. https://doi.org/10.1039/c9gc03287h

[27] Kraus, A., Dierschke, F., Becker, F., Schuhbeck, T., Grassl, H., & Groess, K. (2015, October 13). Method for producing phosphated polycondensation products and the use thereof.

[28] Sulatha, M. S., & Natarajan, U. (2012). Molecular dynamics simulations of PAA–PMA Polyelectrolyte Copolymers in dilute aqueous solution: Chain Conformations and hydration properties. *Industrial & Engineering Chemistry Research*, *51*(33), 10833–10839. https://doi.org/10.1021/ie301244n

[29] Dobrynin, A. V. (2005). Electrostatic persistence length of semiflexible and flexible polyelectrolytes. *Macromolecules*, *38*(22), 9304–9314. https://doi.org/10.1021/ma051353r

[30] Feuz, L., Leermakers, F. A., Textor, M., & Borisov, O. (2005). Bending rigidity and induced persistence length of molecular bottle brushes: a self-consistent-field theory. *Macromolecules*, *38*(21), 8891–8901. https://doi.org/10.1021/ma050871z

[31] Ran, Q., Zhao, H., Shu, X., Zhang, Q., Yang, Y., Liu, J., & Wu, S. (2015). Molecular dynamics study of the effects of calcium ions on the conformational properties of comb-like poly(acrylic acid-co-methyl allyl polyoxyethylene ether). *Computational Materials Science*, *109*, 90–96. https://doi.org/10.1016/j.commatsci.2015.06.020

[32] Chen, J.-H., Lu, L.-Q., Zhao, H.-X., Yang, Y., Shu, X., & Ran, Q.-P. (2019). Conformational properties of comb-shaped polyelectrolytes with negatively charged backbone and neutral side chains studied by a generic coarse-grained bead-and-spring model. Chinese Journal of Polymer Science, 38(4), 371–381. https://doi.org/10.1007/s10118-020-2350-9

[33] Emamyari, S., & Fazli, H. (2018). Single-chain conformational characteristics of comb-like polyelectrolytes: Molecular Dynamics Simulation Study. Macromolecular Research, 27(1), 14–24. https://doi.org/10.1007/s13233-019-7010-y

[34] Tong, K., Song, X., Sun, S., Xu, Y., & Yu, J. (2014). Molecular dynamics study of linear and comb-like polyelectrolytes in aqueous solution: Effect of ca2+ions. Molecular Physics, 112(16), 2176–2183. https://doi.org/10.1080/00268976.2014.893036

[35] Ran, Q., Zhao, H., Shu, X., Zhang, Q., Yang, Y., Liu, J., & Wu, S. (2015). Molecular dynamics study of the effects of calcium ions on the conformational properties of comb-like poly(acrylic acid-co-methyl allyl polyoxyethylene ether). Computational Materials Science, 109, 90–96. https://doi.org/10.1016/j.commatsci.2015.06.020

[36] Sparks, D. J., Romero-González, M. E., El-Taboni, E., Freeman, C. L., Hall, S. A., Kakonyi, G., Swanson, L., Banwart, S. A., & Harding, J. H. (2015). Adsorption of poly acrylic acid onto the surface of calcite: An experimental and simulation study. Physical Chemistry Chemical Physics, 17(41), 27357–27365. https://doi.org/10.1039/c5cp00945f

APPENDICES

APPENDIX A – FREE SOLUTION CONFORMATIONS

APPENDIX A.1 EVOLUTION OF RADIUS OF GYRATION

(a)

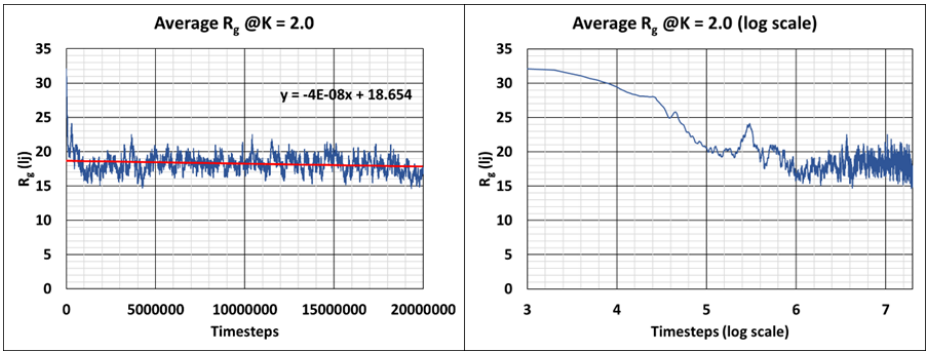

(b)

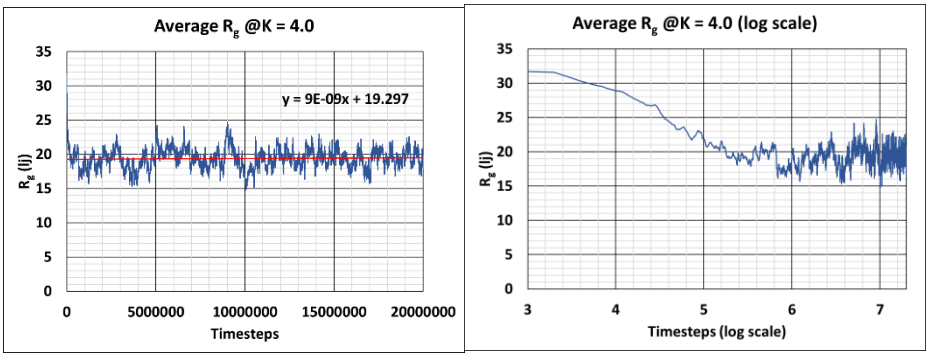

(c)

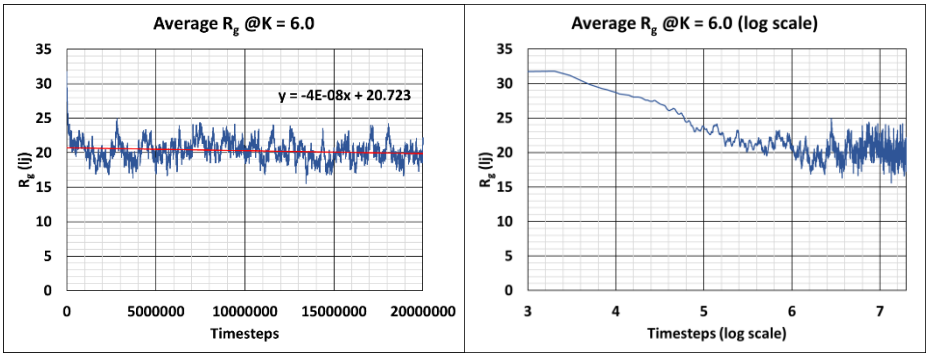

(d)

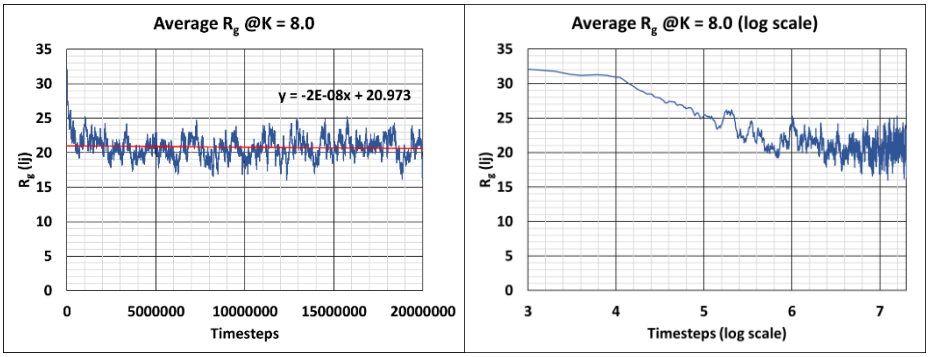

Figure A.1 The average radius of gyration (linear and log scale) for (a) K = 2.0, (b) K = 4.0, (c) K = 6.0 and (d) K = 8.0.

(a)

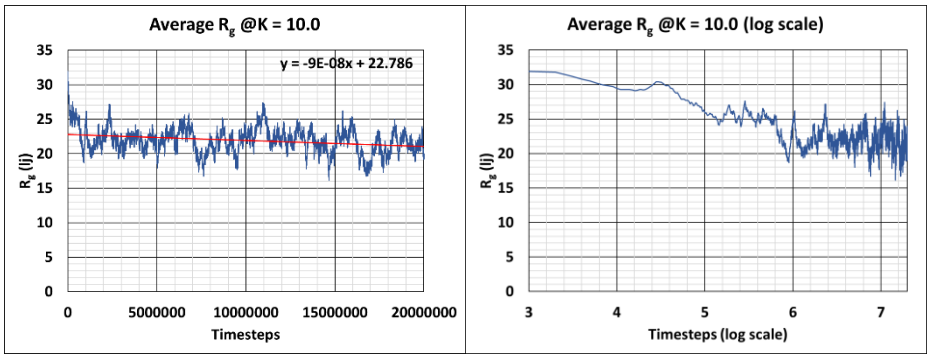

(b)

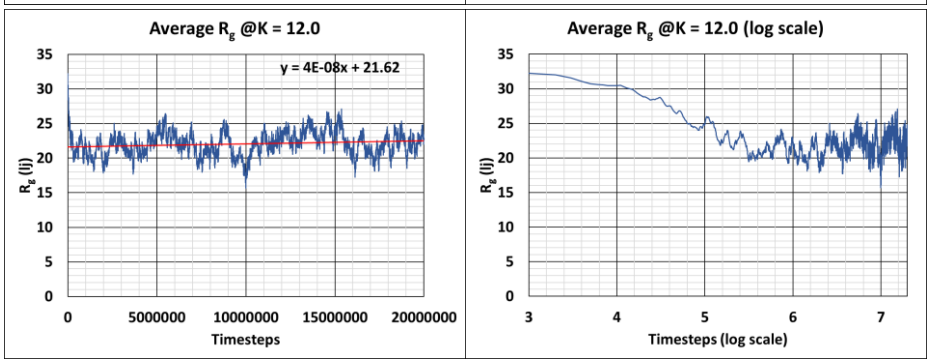

(c)

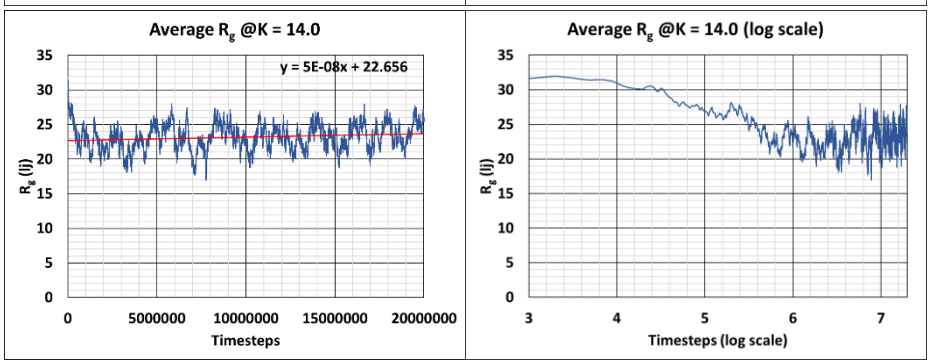

(d)

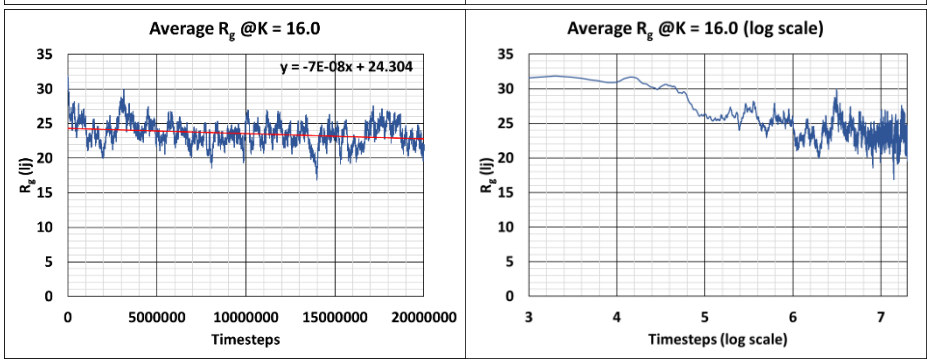

(e)

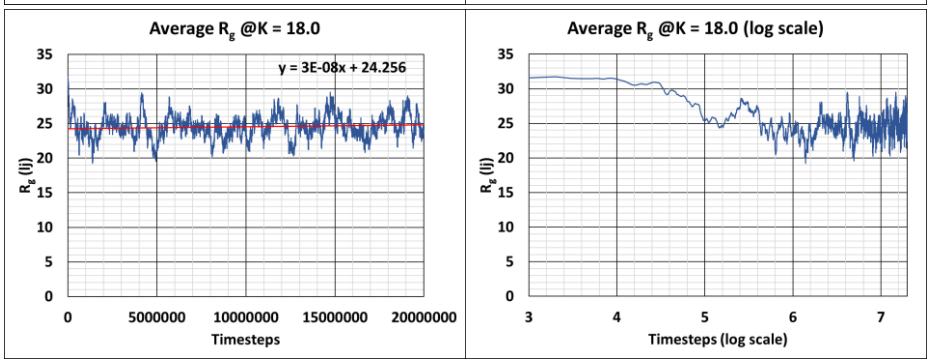

Figure A.2 The average radius of gyration (linear and log scale) for (a) K = 10.0, (b) K = 12.0, (c) K = 14.0, (d) K = 16.0, and (e) K = 18.0.

(a)

(b)

(c)

(d)

(e)

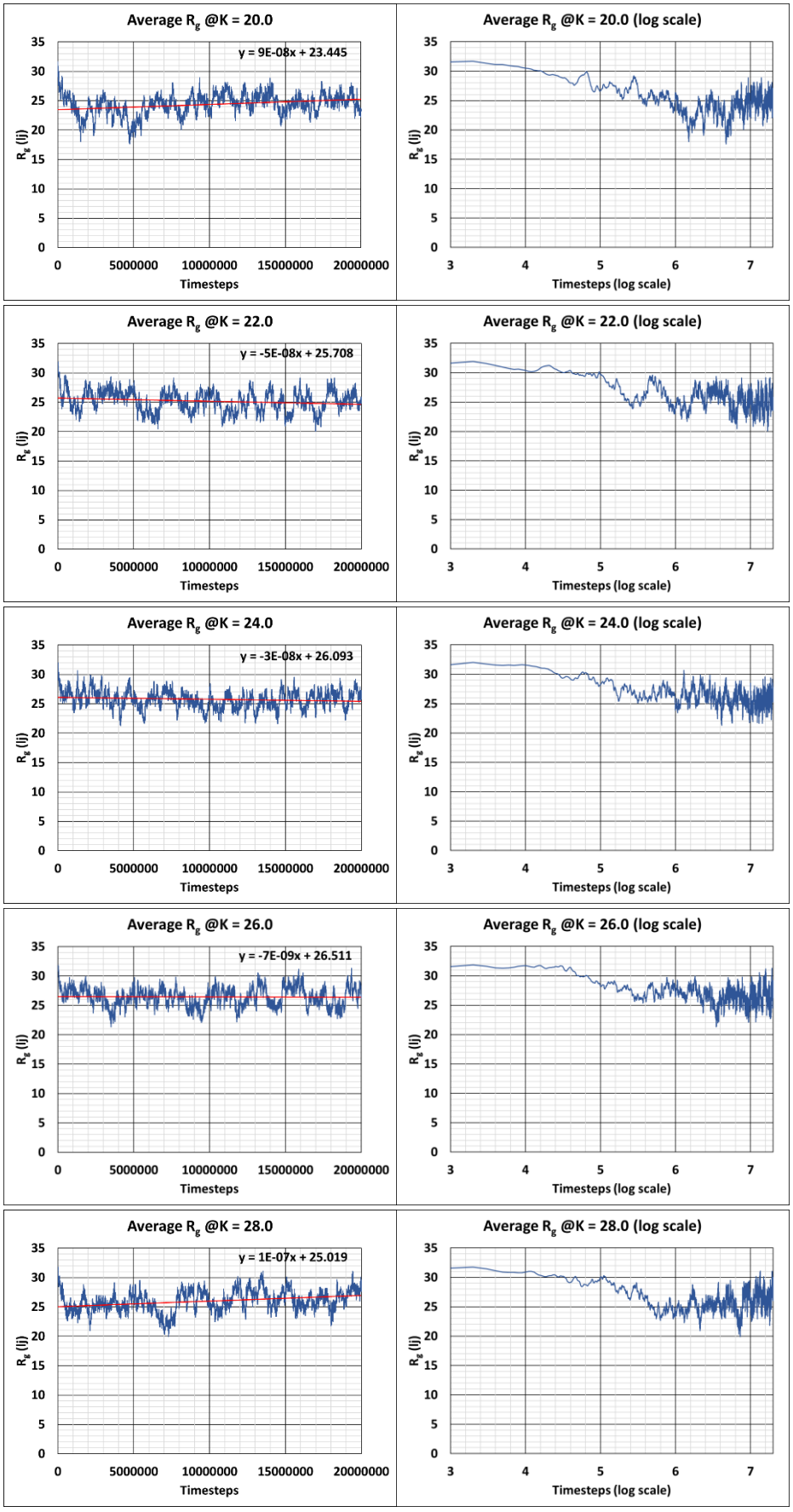

Figure A.3 The average radius of gyration (linear and log scale) for (a) K = 20.0, (b) K = 22.0, (c) K = 24.0, (d) K = 26.0, and (e) K = 28.0.

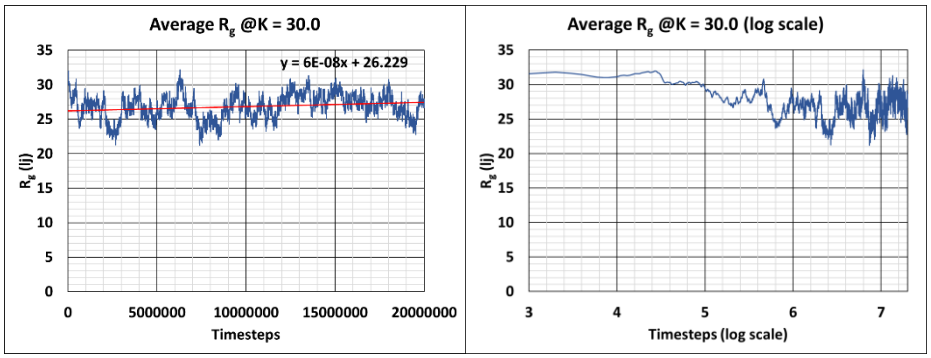

Figure A.4 The average radius of gyration (linear and log scale) for K = 30.0.

APPENDIX A.2 FREE SOLUTION CONFORMATIONS

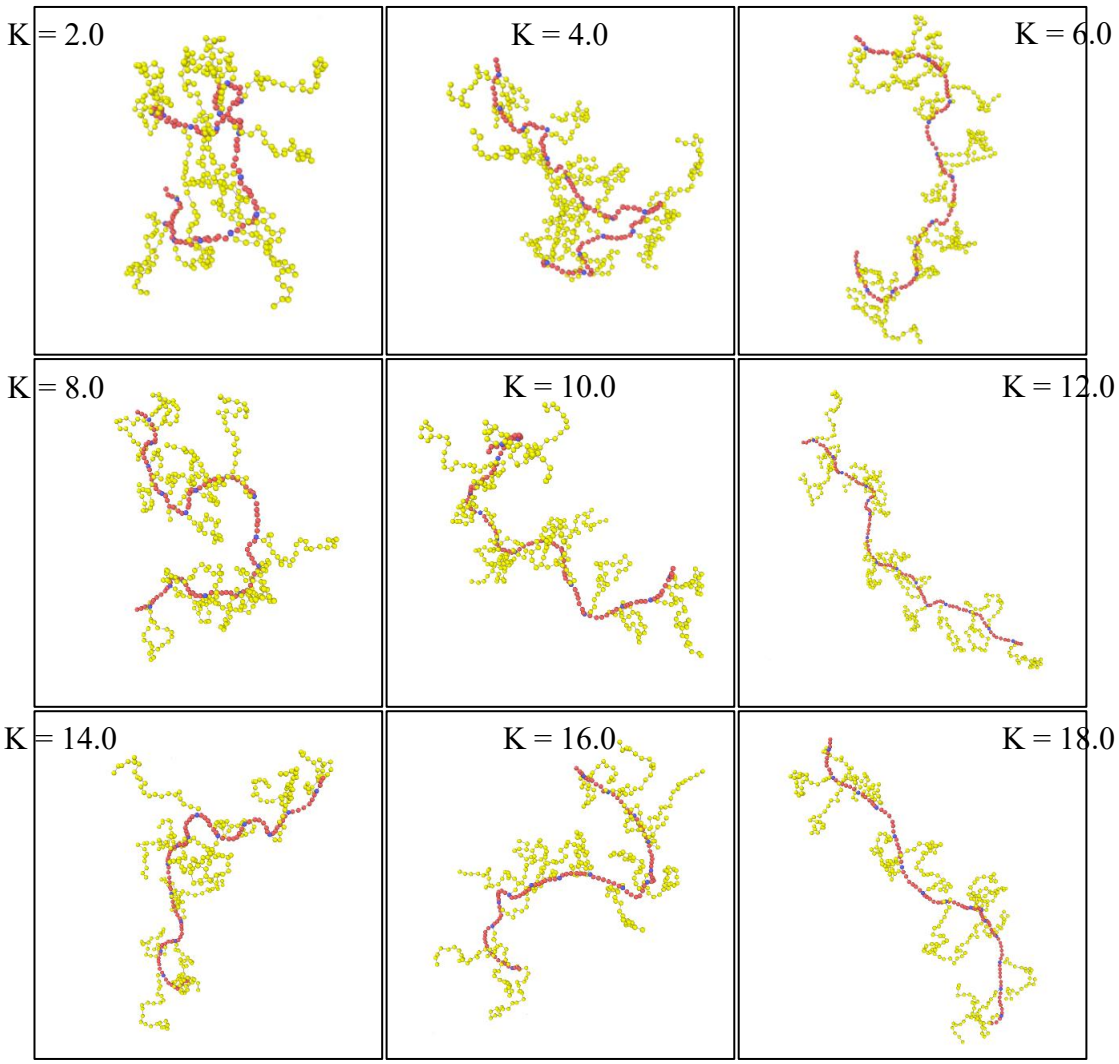

Figure A.5 The simulation snapshots of CP1 copolymers in free solution at $2x10^7$ simulation timesteps.

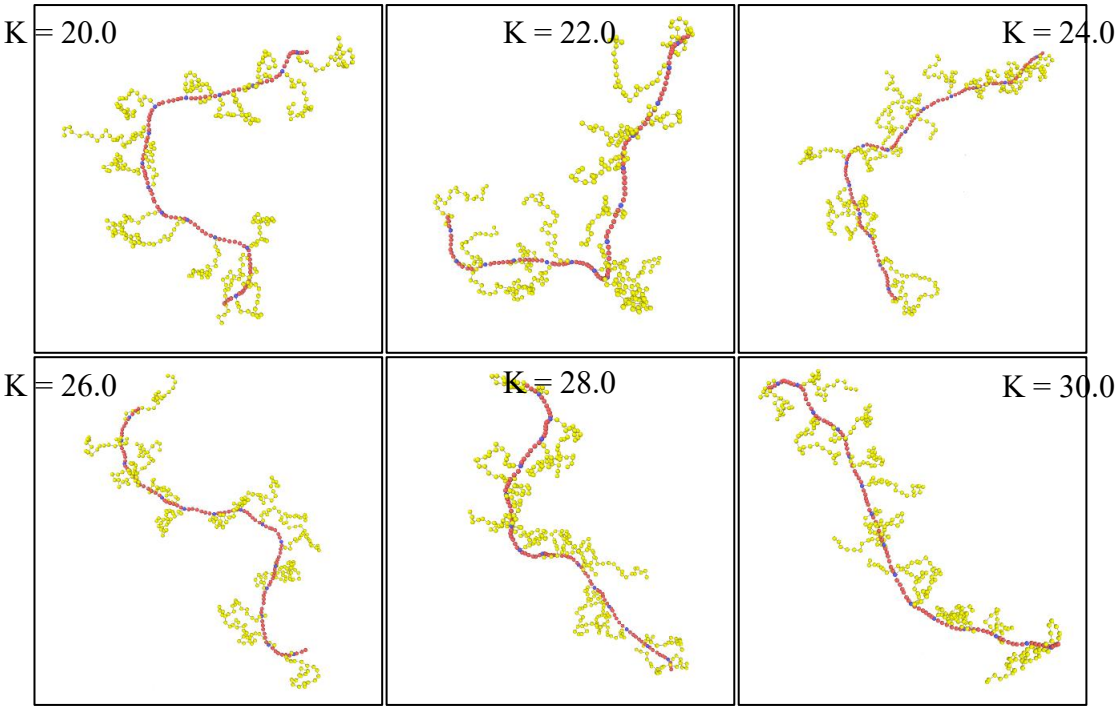

Figure A.6 The simulation snapshots of CP1 copolymers in free solution at $2x10^7$ simulation timesteps.

APPENDIX B – ADSORBED STATE CONFORMATIONS

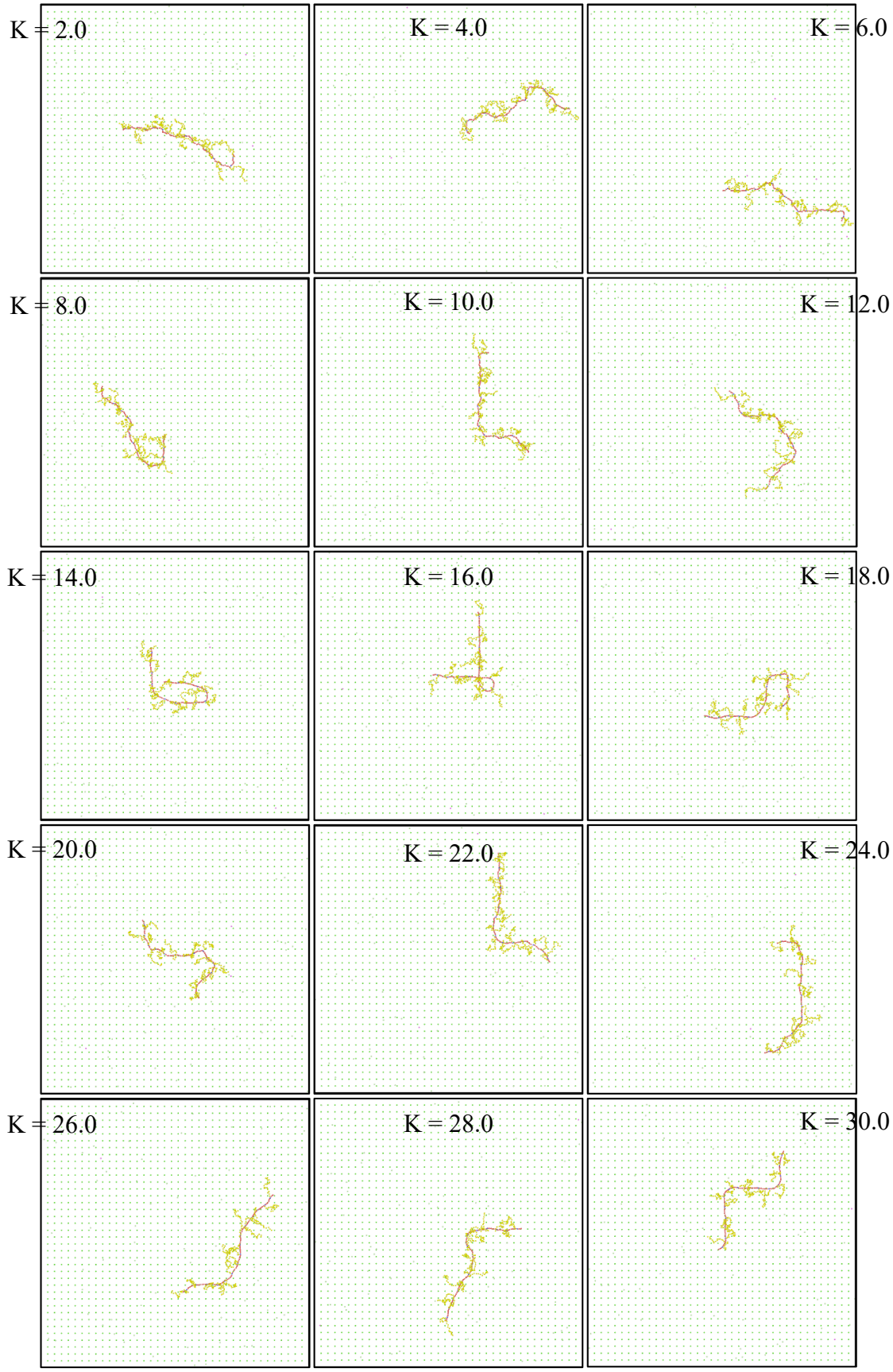

Figure B.1 The top view of CP1 copolymers in adsorbed state at 10^6 simulation timesteps.

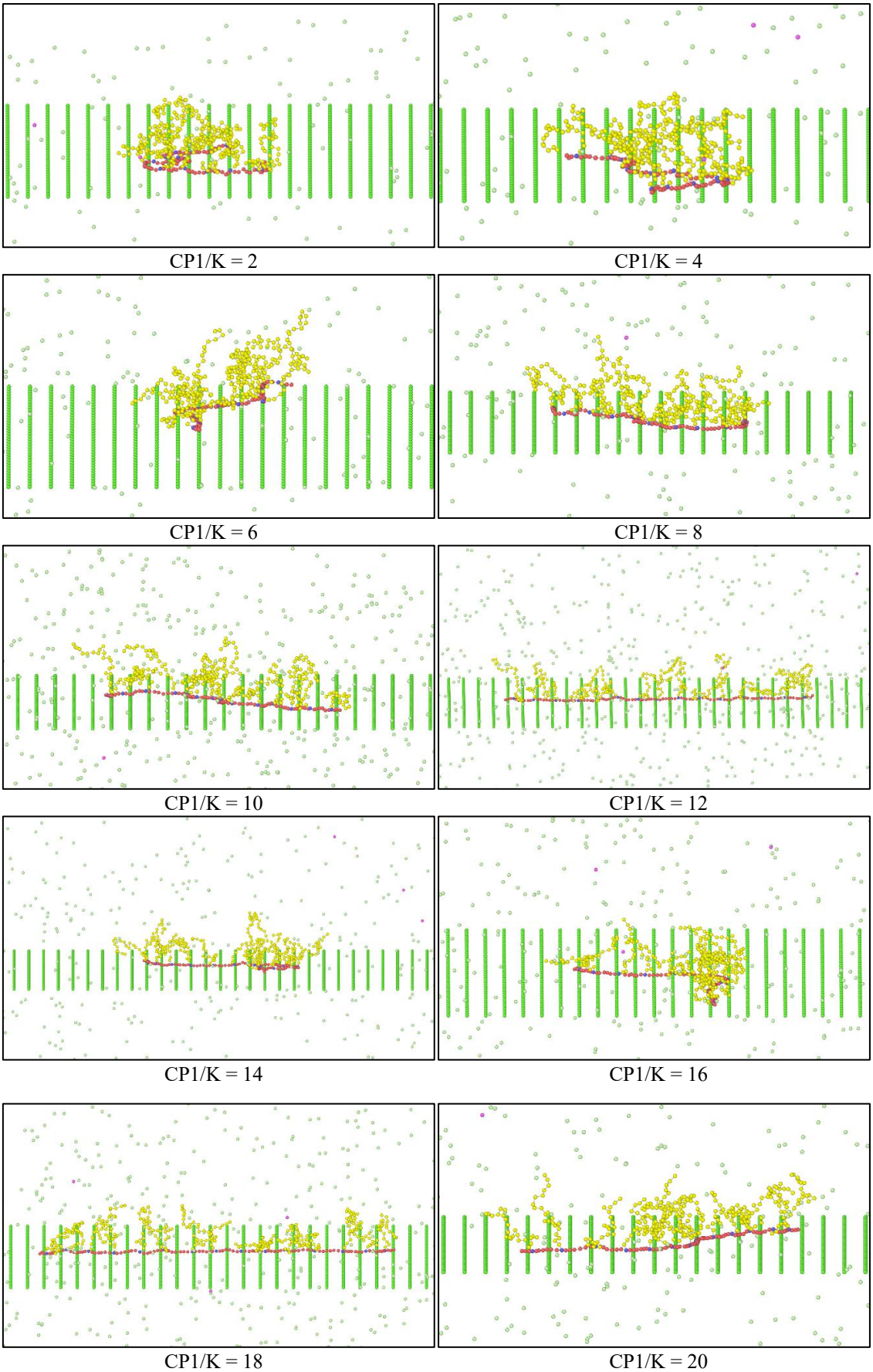

Figure B.2 The simulation snapshots of CP1 copolymers in adsorbed state at 10^6 simulation timesteps.

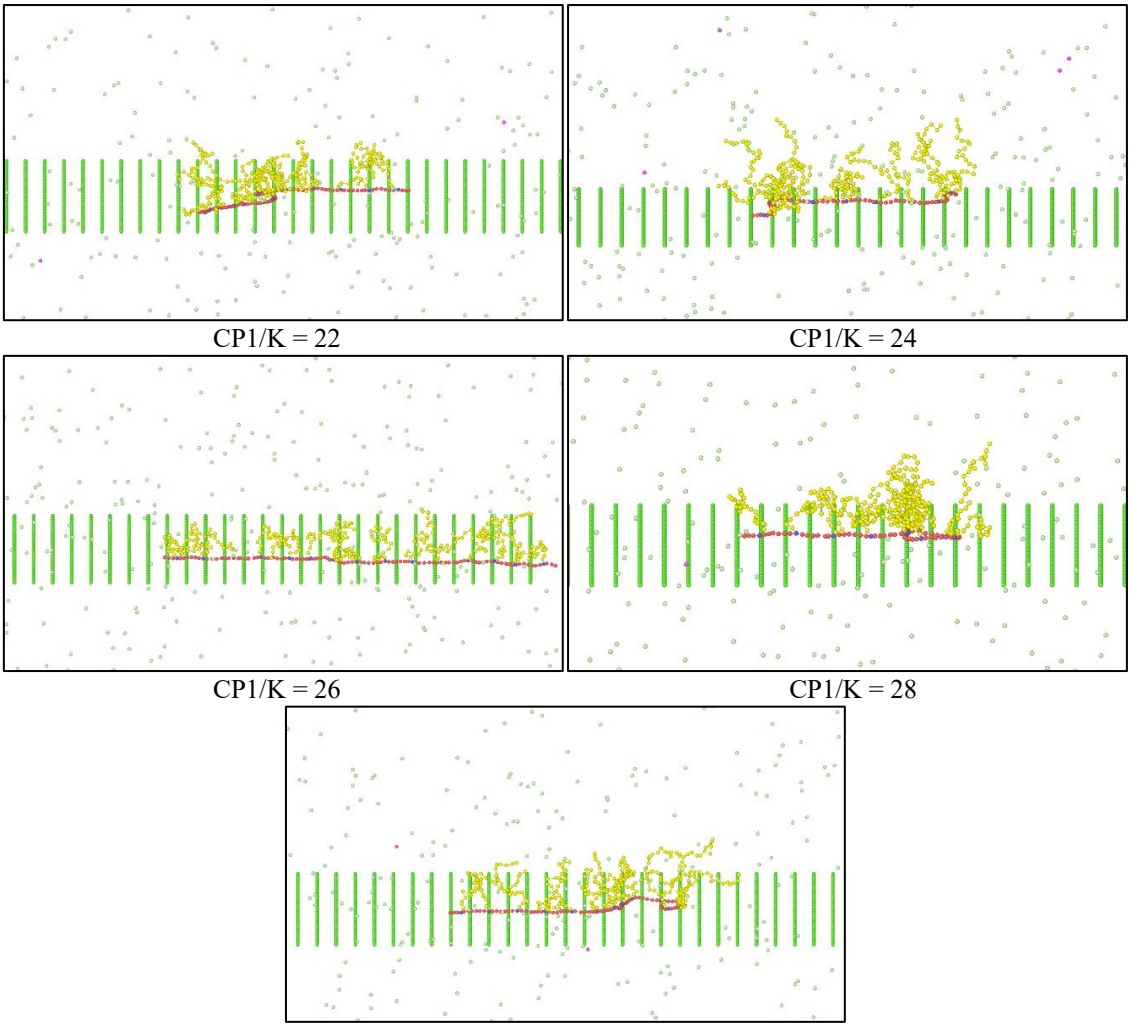

Figure B.3 The simulation snapshots of CP1 copolymers in adsorbed state at 10^6 simulation timesteps.

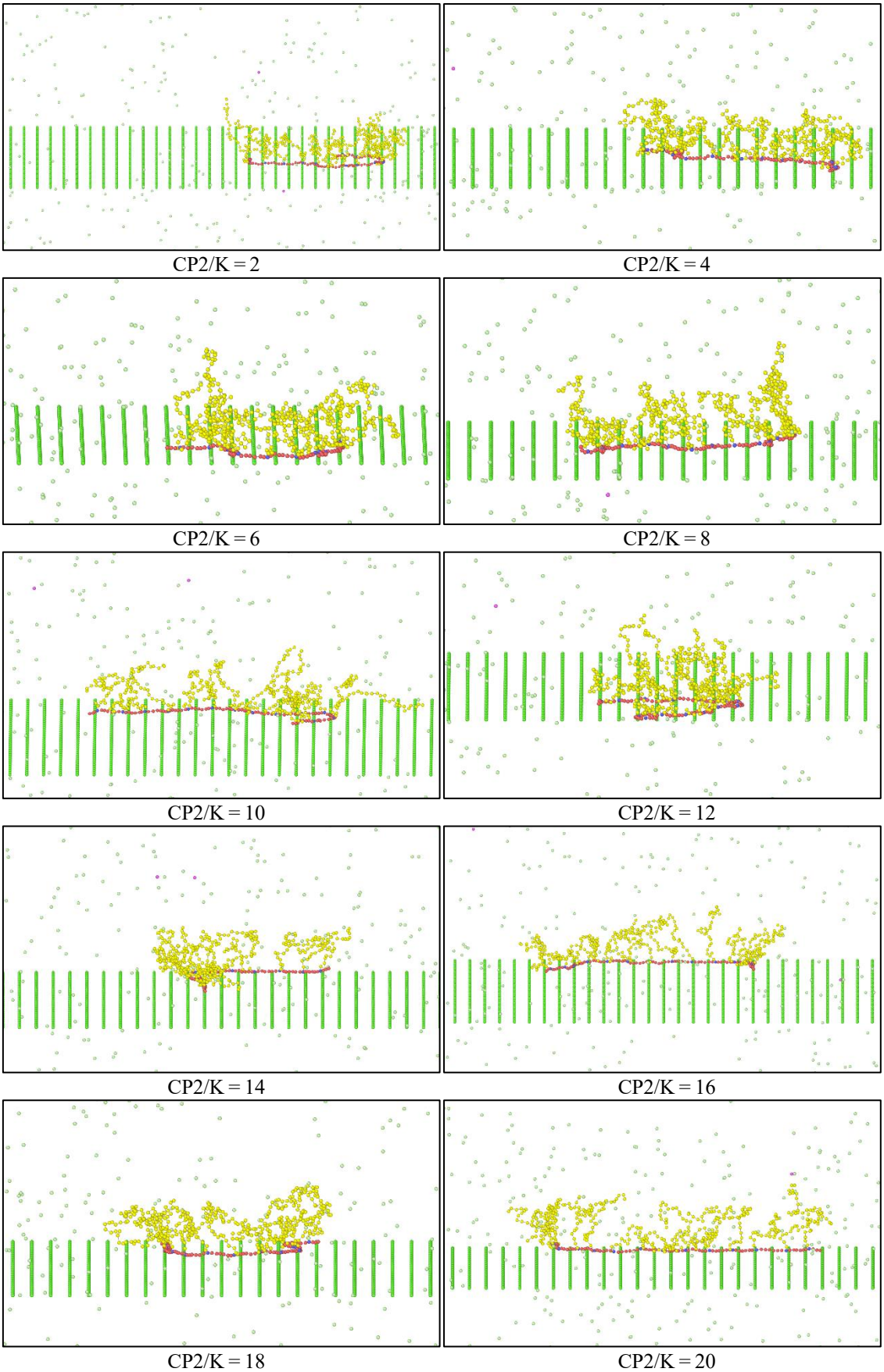

Figure B.4 The simulation snapshots of CP2 copolymers in adsorbed state at 10^6 simulation timesteps.

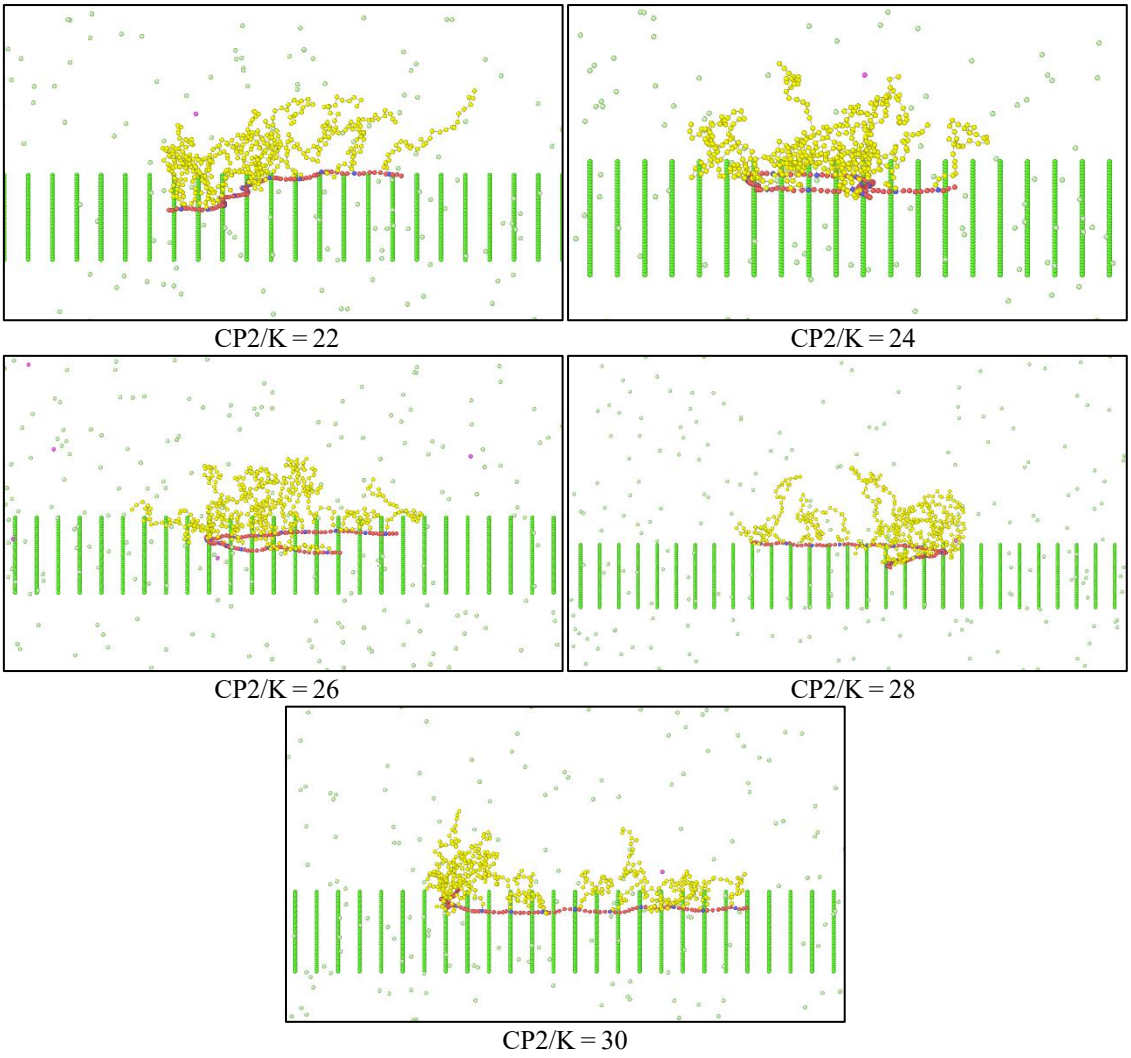

Figure B.5 The simulation snapshots of CP2 copolymers in adsorbed state at 10^6 simulation timesteps.

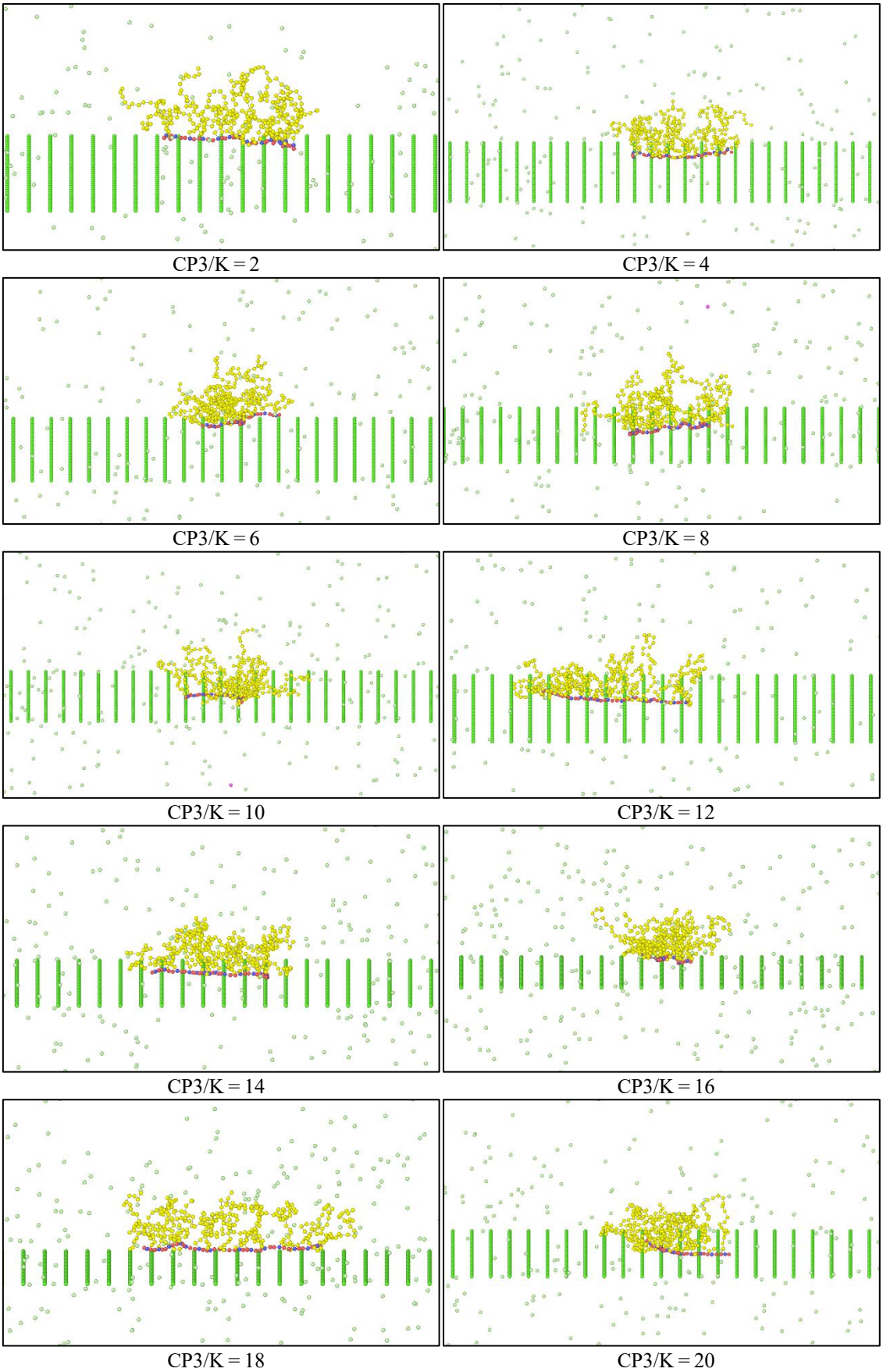

Figure B.6 The simulation snapshots of CP3 copolymers in adsorbed state at 10^6 simulation timesteps.

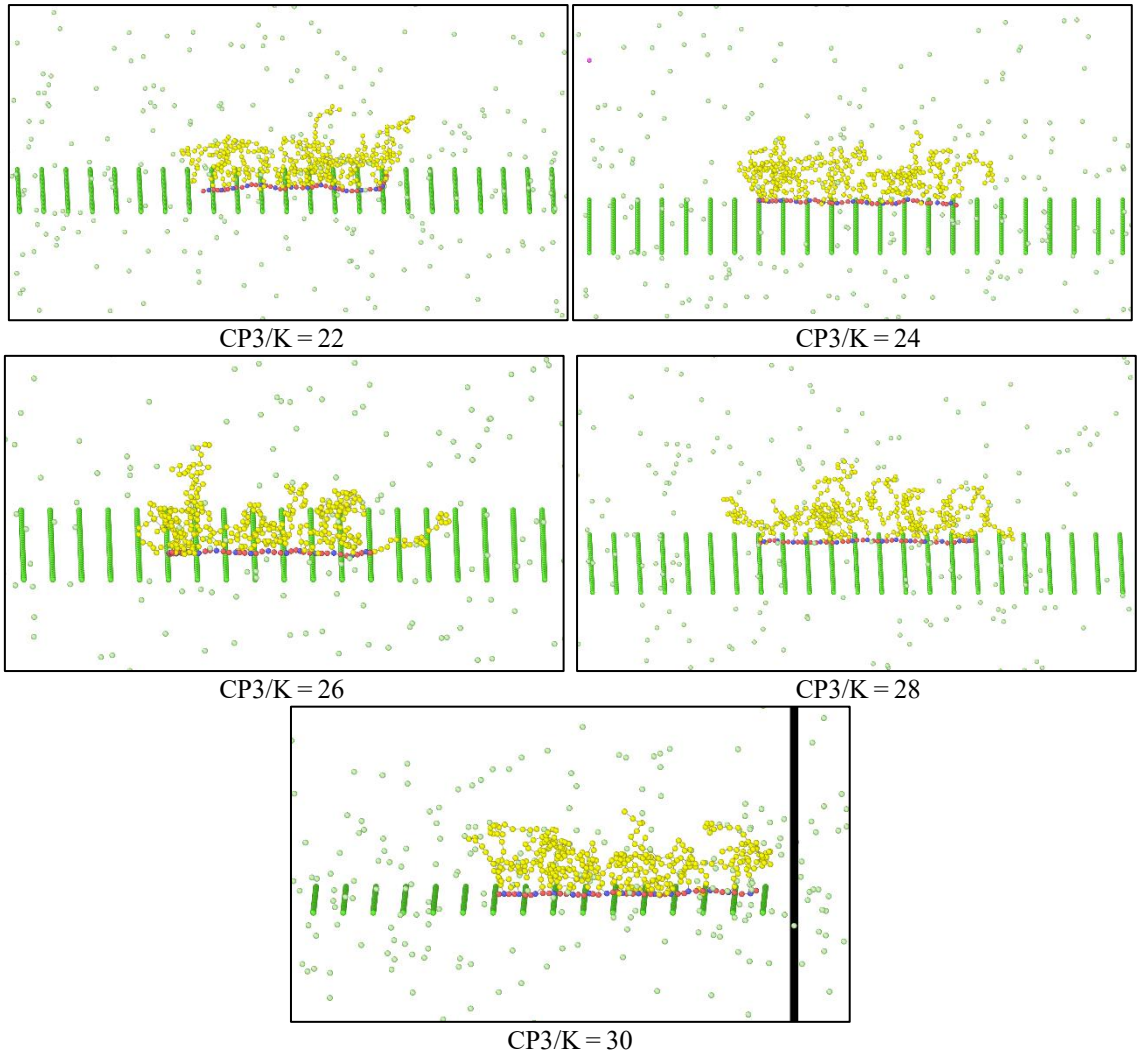

Figure B.7 The simulation snapshots of CP3 copolymers in adsorbed state at 10^6 simulation timesteps.